Extratropical Transition of Tropical Cyclones in a Multiresolution Ensemble of Atmosphere-Only and Fully Coupled Global Climate Models

Alexander J. Baker,[a] Malcolm J. Roberts,[b] Pier Luigi Vidale,[a] Kevin I. Hodges,[a] Jon Seddon,[b] Benoît Vannière,[a] Rein J. Haarsma,[c] Reinhard Schiemann,[a] Dimitris Kapetanakis,[c] Etienne Tourigny,[d] Katja Lohmann,[e] Christopher D. Roberts,[f] and Laurent Terray[g]

[a] National Centre for Atmospheric Science and Department of Meteorology, University of Reading, Reading, Berkshire, United Kingdom
[b] Met Office Hadley Centre, Exeter, Devon, United Kingdom
[c] Koninklijk Nederlands Meteorologisch Instituut, De Bilt, The Netherlands
[d] Earth Sciences Department, Barcelona Supercomputing Center, Barcelona, Spain
[e] Max Planck Institut für Meteorologie, Hamburg, Germany
[f] European Centre for Medium-Range Weather Forecasts, Reading, United Kingdom
[g] Climat, Environnement, Couplages et Incertitudes, Centre Européen de Recherche et de Formation Avancée en Calcul Scientifique (CERFACS), Toulouse, France

ABSTRACT: Tropical cyclones undergo extratropical transition (ET) in every ocean basin. Projected changes in ET frequency under climate change are uncertain and differ between basins, so multimodel studies are required to establish confidence. We used a feature-tracking algorithm to identify tropical cyclones and performed cyclone phase-space analysis to identify ET in an ensemble of atmosphere-only and fully coupled global model simulations, run at various resolutions under historical (1950–2014) and future (2015–50) forcing. Historical simulations were evaluated against five reanalyses for 1979–2018. Considering ET globally, ensemble-mean biases in track and genesis densities are reduced in the North Atlantic and western North Pacific when horizontal resolution is increased from ~100 to ~25 km. At high resolution, multi-reanalysis-mean climatological ET frequencies across most ocean basins as well as basins' seasonal cycles are reproduced better than in low-resolution models. Skill in simulating historical ET interannual variability in the North Atlantic and western North Pacific is ~0.3, which is lower than for all tropical cyclones. Models project an increase in ET frequency in the North Atlantic and a decrease in the western North Pacific. We explain these opposing responses by secular change in ET seasonality and an increase in lower-tropospheric, pre-ET warm-core strength, both of which are largely unique to the North Atlantic. Multi-model consensus about climate change responses is clearer for frequency metrics than for intensity metrics. These results help clarify the role of model resolution in simulating ET and help quantify uncertainty surrounding ET in a warming climate.

KEYWORDS: Extratropical transition; Climatology; General circulation models; Tropical cyclones; Climate change

1. Introduction

The impacts of tropical cyclones are not confined to the tropics. Their post-tropical evolution makes these storms an important natural hazard across the midlatitudes (Baker et al. 2021; Bieli et al. 2019; Evans et al. 2017; Jones et al. 2003; Keller et al. 2019). The poleward propagation of tropical cyclones and the occurrence of extratropical transition (ET) exposes populous regions where risks to life and infrastructure are high—the northeast United States, maritime and eastern Canada, western Europe, and East Asia—to hurricane-force

wind speeds and extreme precipitation (Evans et al. 2017). In the North Atlantic, tropical-origin systems reached northeast North America and Europe almost every year since 1979 (Baker et al. 2021), including recent intense landfalls. For instance, Hurricane Sandy (22–29 October 2012)—the fourth costliest (by inflation-adjusted losses) North Atlantic hurricane yet recorded (Weinkle et al. 2018)—caused devastation across the northeast United States and eastern Canada (Blake et al. 2013). Ex-Hurricane Ophelia (9–15 October 2017) led to loss of life and severe wind damage across Ireland, the United Kingdom, and Scandinavia (Rantanen et al. 2020; Stewart 2018). At midlatitude landfall, both systems were post-tropical, having begun ET, but possessed hurricane-like intensities, the human and economic impacts of which were felt across substantial areas. In the western North Pacific, Typhoon Nabi (29 August–12 September 2005) impacted two-thirds of Japan's prefectures as both a tropical and transitioning cyclone before undergoing cyclolysis over Alaska (Harr et al. 2008). These events, along with the current lack of consensus regarding ET in a changing climate, heighten the urgency with which global studies of historical and near-future post-tropical cyclone activity are needed.

Corresponding author: Alexander J. Baker, alexander.baker@reading.ac.uk

Tropical cyclones undergo ET in every ocean basin (Hart and Evans 2001; Studholme et al. 2015; Wood and Ritchie 2014; Zarzycki et al. 2017), but pronounced interannual variability (Baker et al. 2021) and basin-to-basin differences (Bieli et al. 2019) exist. Transitioning cyclones are also known to influence the large-scale circulation, such as Hurricane Debbie in 1982 (Laurila et al. 2019), and excite or amplify downstream Rossby waves (Evans et al. 2017; Jones et al. 2003; Keller et al. 2019; Michaelis and Lackmann 2019). These cyclone–wave interactions influence downstream weather (Grams and Blumer 2015; Keller et al. 2019). Of those cyclones that undergo ET, an appreciable proportion reintensify under favorable environmental conditions, where appropriate phasing between the transitioning cyclone and the upper-tropospheric flow pattern enhances baroclinic instability (Keller et al. 2019). During and after ET, baroclinicity (Evans et al. 2017) and diabatic heating (Rantanen et al. 2020) may reintensify post-tropical cyclones.

Over the period of 1979–2018, statistically significant positive trends in the frequency of North Atlantic ET events exist in several, but not all, reanalysis datasets (Baker et al. 2021). Existing climate model projections underline the plausibility of increased tropical and post-tropical cyclone activity in the midlatitudes in response to anthropogenic warming. There is evidence that more frequent ET events may occur in the future in the North Atlantic (Baatsen et al. 2015; Haarsma et al. 2013; Liu et al. 2017; Michaelis and Lackmann 2019) and western North Pacific (Bieli et al. 2020) ocean basins, but no consensus yet exists across studies, modeling campaigns, and methodologies. Moreover, best-track data limitations, which are well documented (Chang and Guo 2007; Delgado et al. 2018; Hagen et al. 2012; Vecchi and Knutson 2008), engender substantial uncertainty in observed trends (Lanzante 2019; Moon et al. 2019). Additionally, natural, multidecadal variability in tropical cyclone frequency is yet to be accounted for (Knutson et al. 2020). Although global climate models project reduced frequencies of tropical cyclones, more intense tropical cyclones are expected in response to twenty-first-century warming (Knutson et al. 2020), potentially allowing a higher proportion of cyclones to survive cooler midlatitude sea surface temperatures experienced prior to and during ET (Michaelis and Lackmann 2019). Other factors, particularly changes in shear, will also be important, with current evidence suggesting that these will undergo ET-favorable future changes (Jung and Lackmann 2021; Liu et al. 2017; Michaelis and Lackmann 2021). Increased future ET event frequency is also consistent with the projected expansion of tropical cyclone genesis regions (Studholme et al. 2022), potentially reducing the mean displacement cyclones must undergo prior to midlatitude ET. Together, these changes imply an increase in post-tropical cyclone impacts across populated midlatitude regions, and idealized experiments suggest an increase in ET-related, high-impact weather across Europe (Jung and Lackmann 2021), where our understanding of historical risks is developing (Baker et al. 2021). Studies of historical and future model simulations are therefore needed to assess both contemporary risk and future changes more comprehensively.

One aspect of climate model evaluation important for both tropical and extratropical cyclones is understanding the role of horizontal resolution in simulated climates, prompted by recent developments in high-performance computing and data management facilities. With increases in model resolution to approximately 25 km, improved fidelity is anticipated for many synoptic phenomena, particularly tropical and midlatitude cyclones, which ultimately feed back onto the large scale. Recent studies have now firmly established that increasing model resolution improves simulated tropical cyclone frequency statistics across most ocean basins (Manganello et al. 2019; Roberts et al. 2020a), leads to a more realistic global spatial distribution (Roberts et al. 2020a, 2015; Strachan et al. 2013), and results in more realistic simulated warm-core vertical structures (Vannière et al. 2020). Moreover, model resolution is a key constraint on the intensity which simulated cyclones may reach (Davis 2018). It is anticipated that atmospheric resolutions of ~50 km or finer (~0.25° ocean-model resolution) will yield improvement in the simulation of post-tropical cyclones and ET (Haarsma 2021). However, no systematic multimodel studies of ET have been undertaken, and the impact of increasing model resolution (atmosphere and ocean) on simulated ET is also yet to be quantified. We address these issues in this paper using model simulations from phase 6 of the Coupled Model Intercomparison Project (CMIP6), which follow an experimental protocol designed to isolate the impacts of changes in model resolution.

In this study of the representation of tropical cyclones undergoing ET across a multimodel ensemble, we focus on climatological statistics, interannual variability, and cyclone structure and intensity. These analyses are centered around two questions. What is the impact of increasing model atmospheric resolution on simulated ET? What changes in ET metrics under climate change are consistent across models? This paper continues in section 2 with a description of the model and reanalysis data as well as the cyclone tracking and analysis methodologies. Our results are presented in section 3 and our conclusions are summarized, with further discussion, in section 4.

2. Data and methodology

a. Reanalysis data

Tropical cyclone best-track datasets are not well suited to analysis of cyclones undergoing ET because there are known heterogeneities within individual datasets (Barcikowska et al. 2012; Chu et al. 2002; Kossin et al. 2007; Vecchi and Knutson 2008, 2011), especially for storms' post-tropical stages, undercounting biases (Chang and Guo 2007; Delgado et al. 2018; Hagen et al. 2012), and differences between operational centers' data collection methodologies (Hodges et al. 2017; Schreck et al. 2014). We therefore evaluated model simulations against five global reanalyses (Table 1): the European Centre for Medium-Range Weather Forecasts (ECMWF) interim reanalysis (ERA-Interim, herein ERAI; Dee et al. 2011) and ERA5 (Hersbach et al. 2020); the Japanese 55-year Reanalysis (JRA-55; Kobayashi et al. 2015); the National Aeronautics and Space Administration's Modern-Era Retrospective Analysis for Research and Applications version 2 (MERRA-2; Molod et al. 2015); and the combined National Centers for Environmental

TABLE 1. Reanalyses. Atmospheric mesh spacing at 50°N (km) is given in parentheses. 3(4)D-Var: 3(4)D variational data assimilation; GSI: Grid-point Statistical Interpolation; IAU: Incremental Analysis Update. The representations of tropical and post-tropical cyclones in these reanalyses were evaluated by Hodges et al. (2017) and Baker et al. (2021), respectively. Annual-mean global sample sizes (cyclones per year) for all tropical cyclones undergoing ET for each reanalysis are given as n_{NH}, n_{SH}.

Reanalysis	Analysis period	Analysis grid	Model resolution (grid spacing)	Data assimilation	Sample size (n_{NH}, n_{SH})
ERAI	1979–2017	512 × 256	TL255L60 (80 km)	4D-Var	35.4, 37.0
ERA5	1979–2018	1140 × 721	T639L137 (33 km)	4D-Var	40.4, 38.2
JRA-55	1959–2014	288 × 145	TL319L60 (55 km)	4D-Var	35.6, 44.3
MERRA-2	1980–2017	576 × 361	Cubed sphere (50 km)	3D-Var + GSI + IAU	35.7, 28.6
NCEP	1979–2016	720 × 361	T382L64 (38 km)	3D-Var + GSI	36.2, 30.6

Prediction Climate Forecast System Reanalysis and Climate Forecast System version 2 dataset (NCEP; Saha et al. 2014)—the sole fully coupled (atmosphere, ocean, land surface, and sea ice) reanalysis used herein. Between reanalyses, differing forecast model formulations and resolutions (horizontal and vertical), as well as data assimilation schemes lead to differences in the representation of tropical cyclone vertical structure, which was examined by Hodges et al. (2017). Baker et al. (2021) found that interannual variability in the number ET events is well correlated between reanalyses, but the percentage of tropical cyclones undergoing ET agrees less well between reanalyses on the interannual time scale. It is therefore necessary to consider multiple reanalyses as an observation-based reference, against which models may be evaluated.

b. The multiresolution PRIMAVERA model ensemble

We evaluated CMIP6 High-Resolution Model Intercomparison Project (HighResMIP; Haarsma et al. 2016) historical and future atmosphere-only (tier 1 and tier 3, respectively), including interaction with the land surface, and fully coupled (tier 2) simulations from five global climate models (Table 2): CNRM-CM6.1 (Voldoire et al. 2019), EC-Earth3P (Haarsma et al. 2020), ECMWF-IFS (cycle 43r1; Roberts et al. 2018), HadGEM3-GC3.1 (Roberts et al. 2019; Williams et al. 2018), and MPI-ESM1.2 (Gutjahr et al. 2019). Each model participated in the European Commission Horizon2020-funded project PRIMAVERA (Process-Based Climate Simulation: Advances in High-Resolution Modeling and European Climate Risk Assessments; https://primavera-h2020.eu). Historical (1950–2014) and future (2015–50) atmosphere-only experiments are termed "highresSST-present" and "highresSST-future," respectively, and fully coupled experiments are termed "hist-1950" and "highres-future," respectively. Historical highresSST-present simulations were forced by HadISST2 daily sea surface temperature (SST) at a resolution of 0.25° interpolated to each model's grid (no ocean mixed-layer model). Out to 2050, highresSST-future simulations were forced according to representative concentration pathway 8.5 (RCP8.5). (Use of RCP8.5 allowed modeling centers to begin their model simulations before Shared Socioeconomic Pathways scenarios became available.) In HighResMIP, future simulations were performed with all models except ECMWF-IFS. The rate of projected sea surface temperature (SST) warming was derived from an ensemble mean of CMIP5, with interannual variability derived from the historical period 1950–2014 (Haarsma et al. 2016).

Under the HighResMIP experimental protocol, minimal changes in model-tuning parameters were made between low- and high-resolution integrations to ensure that resolution-sensitivity studies were not confounded by substantial differences in model configurations between resolutions (Haarsma et al. 2016). Between low- and high-resolution configurations, no model physics changes were made to the atmospheric components

TABLE 2. The PRIMAVERA (HighResMIP) model ensemble. NEMO: Nucleus for European Modeling of the Ocean. MPIOM: Max Plank Institute Ocean Model. SISL: semi-implicit, semi-Lagrangian. For fully coupled simulations, the LL and HH configurations of HadGEM3-GC3.1 were also included; LL denotes low-resolution atmosphere and low-resolution (1°) ocean, and HH denotes high-resolution atmosphere and high-resolution (1/12°) ocean. Atmosphere mesh spacing is given for 50°N. Sample sizes for all tropical cyclones undergoing ET across this ensemble are given in Table 3. DOIs for each simulation are listed at https://www.primavera-h2020.eu/modelling/.

Model name	Atmospheric model	Ocean model	Atmospheric dynamical core	Resolution nomenclature	Atmospheric resolution	Atmospheric mesh spacing
CNRM-CM6.1	ARPEGE6.3	NEMO	Spectral (linear, reduced Gaussian)	LR; HR	TL127; TL359	142; 50 km
EC-Earth3P	IFS cyc36r4	NEMO	Spectral (linear, reduced Gaussian)	LR; HR	TL255; TL511	71; 36 km
ECMWF-IFS	IFS cyc43r1	NEMO3.4	Spectral (cubic octahedral; reduced Gaussian)	LR; HR	Tco199; Tco399	50; 25 km
HadGEM3-GC3.1	MetUM	NEMO	Grid point (SISL)	LM (LL); MM; HM (HH)	N96; N216; N512	135; 60; 25 km
MPI-ESM1.2	ECHAM6.3	MPIOM1.63	Spectral (triangular; Gaussian)	HR; XR	T127; T255	67; 34 km

of CNRM-CM6.1 and EC-Earth3P, but minor adjustments were made to a single parameter in ECMWF-IFS (related to net surface energy balance), HadGEM3-GC3.1 (related to quasi-biennial oscillation period), and MPI-ESM1.2 (related to numerical stability). For the ocean model in coupled configurations, one key difference is the effects of mesoscale eddies are parameterized at low resolution (~1°) but partially resolved at high resolution (~0.25°) (e.g., Roberts et al. 2018, 2019). For all models, shorter dynamical time steps were used in the high-resolution integrations to ensure numerical stability. The effective resolutions of the high-resolution model configurations, measured by kinetic energy spectra, resolve synoptic-scale dynamics (Klaver et al. 2020). Since this study concerns cyclone translation from the tropics to the extratropics, resolutions are given as a model's regular mesh spacing at a latitude of 50° (Table 2). For convenience, we refer to resolutions nominally (i.e., "low" or "high") as well as quantitatively, where necessary. A single ensemble member was analyzed at each resolution for both the atmosphere-only and fully coupled experiments.

c. Lagrangian tropical cyclone tracking

To identify and track the evolution of tropical cyclones, we used the objective feature-tracking algorithm (TRACK) of Hodges (1995), a well-established tool for identifying cyclones in reanalyses (Hodges et al. 2017) and model simulations (Roberts et al. 2020a). The TRACK algorithm was applied to 6-hourly relative vorticity, computed from the zonal and meridional wind fields, which was vertically averaged over the 850-, 700- and 600-hPa levels and spectrally filtered. (Upper-level vorticity is used in subsequent identification.) Filtering to the T6–T63 spectral band removes both large, planetary scales (total wavenumbers 0–5) and small-scale noise (total wavenumbers > 63). Vorticity maxima exceeding 0.5×10^{-5} s^{-1} (in the Northern Hemisphere; scaled by -1 in the Southern Hemisphere) were identified, initialized into tracks using a nearest-neighbor approach, and subsequently refined by minimizing a cost function for track smoothness, subject to adaptive constraints on track displacement and smoothness (Hodges 1995, 1999). The use of vertically averaged vorticity improves temporal coherence in instances where vorticity maxima shift between levels (Hodges et al. 2017).

Cyclone-centered sampling of meteorological fields along cyclone tracks was performed to detect warm-core structures and measure cyclone intensities, following Hodges et al. (2017). For warm-core identification, the T63-truncated vorticity data on seven levels covering 850–250 hPa were added to tracks by recursively searching for a vorticity maximum at each level using the previous level's maximum as the starting point for a steepest-ascent maximization applied to the B-spline-interpolated field. A search radius of 5° was used, centered on each level's maximum. For the Southern Hemisphere, fields were scaled by -1. To quantify cyclone intensity, mean sea level pressure minima within a radius of 5° and 925-hPa and 10-m wind speed maxima within a radius of 6° of the storm center were sampled from reanalysis or model-output fields at their native, nontruncated resolutions. (All radii are geodesic.)

Following Hodges et al. (2017), objective identification of tropical cyclones adhered to the following criteria:

- cyclogenesis equatorward of 30°N,
- total cyclone lifetime must exceed two days,
- T63 relative vorticity at 850 hPa must exceed 6×10^{-5} s^{-1},
- T63 relative vorticity center must exist at each level between 850 and 250 hPa to indicate a coherent vertical structure, and
- T63 relative vorticity decrease with increasing height between 850 and 250 hPa by at least 6×10^{-5} s^{-1} to indicate the presence of a warm core.

The three T63 relative vorticity criteria must also be jointly attained for at least four consecutive time steps (i.e., one day) over ocean only. Together, these criteria minimize inclusion of spurious short-lived or relatively weak vorticity features. The same criteria were used for each reanalysis and model simulation and across all ocean basins.

Crucial to our analyses, vorticity-based tracking and post-tracking identification of tropical cyclones yields longer cyclone life cycles (compared with central pressure–based algorithms and methodologies where identification is performed during tracking), which allows for objective analysis of post-tropical storm evolution (Hodges et al. 2017). A comparison of TRACK results with results from a different tracking algorithm, which does not capture the full life cycle, demonstrates this advantage of vorticity-based tracking (see section S1.1 and Fig. S1 in the online supplemental material). In addition, filtering gridded data to a common spectral truncation, rather than tuning the cyclone tracking algorithm to a given dataset, allows both inter-model and inter-resolution comparisons that are not complicated by methodological differences (Hodges et al. 2017). Applying TRACK to a reanalysis globally, as described here, identifies ~30 000 tropical vortices per year. Of these, ~8000 per year have a lifetime that exceeds two days and are retained; of these, ~120 per year exhibit the warm-core structure of a tropical cyclone (Vannière et al. 2020). Our study is based on recently published tropical cyclone track datasets, derived using a consistent methodology (Roberts et al. 2020a,b). Sample sizes for all tropical cyclones undergoing ET are given in Table 3. Finally, spatial track statistics—track and genesis densities—were computed using spherical kernel estimators, following Hodges (1996).

d. Cyclone phase space analysis

The temporal evolution of cyclone structure, including identifying ET, is quantifiable by analysis of a cyclone's thermal wind fields (Hart 2003; Hart and Evans 2001). So-called cyclone phase space analysis involves three parameters: the thermal axisymmetry of the cyclone [B; Eq. (1)] and the lower- [T_L; Eq. (2)] and upper-tropospheric [T_U; Eq. (3)] cyclone-relative thermal winds. In this study, these parameters were computed using 6-hourly data for all reanalyses and climate models. Here B is defined as

$$B = h(\overline{Z_{600} - Z_{925}}|_R - \overline{Z_{600} - Z_{925}}|_L), \quad (1)$$

where $h = 1$ for the Northern Hemisphere and -1 for the Southern Hemisphere, Z_p is geopotential height (m) at level p

TABLE 3. Annual-mean global sample sizes (cyclones per year) for all tropical cyclones undergoing ET in each model simulation, given as n_{NH}, n_{SH}.

Model name	Atmosphere-only		Fully coupled	
	highresSST-present	highresSST-future	hist-1950	highres-future
CNRM-CM6.1	42.3, 52.0	41.0, 47.5	43.4, 45.8	40.1, 39.4
CNRM-CM6.1-HR	47.9, 55.9	46.7, 51.5	50.0, 49.6	46.8, 42.3
EC-Earth3P	19.2, 29.3	20.1, 28.9	19.9, 27.6	19.1, 24.0
EC-Earth3P-HR	30.1, 32.1	29.1, 29.4	26.6, 28.8	26.8, 27.8
ECMWF-IFS-LR	34.7, 41.6	—	29.6, 41.5	—
ECMWF-IFS-HR	39.8, 44.6	—	34.5, 41.7	—
HadGEM3-GC3.1-LL	—	—	28.4, 38.7	28.6, 36.3
HadGEM3-GC3.1-LM	36.3, 50.0	36.5, 50.7	—	—
HadGEM3-GC3.1-MM	60.1, 68.8	60.9, 65.0	55.0, 56.0	53.2, 53.4
HadGEM3-GC3.1-HM	63.8, 69.0	63.1, 64.6	58.1, 56.4	58.9, 54.3
HadGEM3-GC3.1-HH	—	—	63.4, 56.2	60.1, 52.9
MPI-ESM1.2-HR	10.5, 16.0	9.4, 14.5	11.4, 16.9	10.4, 15.5
MPI-ESM1.2-XR	10.1, 17.0	9.6, 15.0	11.1, 17.4	10.1, 14.9

(isobaric; hPa), and subscript R and L denote the right- and left-hand semicircles, respectively, relative to the cyclone's displacement direction. In this study, we followed the majority of previous research (Bieli et al. 2019, 2020; Dekker et al. 2018; Hart 2003; Liu et al. 2017; Studholme et al. 2015) and defined thermal axisymmetry (i.e., nonfrontal) as $B < 10$ and asymmetry (i.e., frontal) as $B \geq 10$ m. To compute T_L and T_U between isobaric surfaces, Hart (2003) used the slope of the linear regression between ΔZ and $\ln p$ as the derivative of ΔZ relative to $\ln p$ to determine the mean ΔZ over a given pressure range. However, to ensure consistency between phase-space parameters computed from reanalyses and model output, and to account for the different pressure levels on which reanalysis and model data are available, it was necessary to adopt a three-level procedure, following recent studies (Bieli et al. 2019, 2020; Liu et al. 2017; Studholme et al. 2015). Here, T_L (925–600 hPa) and T_U (600–250 hPa) are defined as vertical derivatives of the horizontal geopotential height gradient:

$$T_L \equiv -|V_T^L| = \frac{\partial (\Delta Z)}{\partial \ln p}\bigg|_{925\,hPa}^{600\,hPa}, \quad (2)$$

$$T_U \equiv -|V_T^U| = \frac{\partial (\Delta Z)}{\partial \ln p}\bigg|_{600\,hPa}^{250\,hPa}, \quad (3)$$

where p is pressure and $\Delta Z = Z_{max} - Z_{min}$, where Z_{max} and Z_{min} are the maximum and minimum geopotential height, respectively, at a given level within a 5° radius of the cyclone center. Positive T_L or T_U indicates the presence of a warm core in the upper or lower troposphere, respectively; negative values indicate a cold core. A deep warm- or cold-core structure is identified where T_L and T_U have the same sign. We performed phase-space analysis for all reanalyses (section 2a) and all PRIMAVERA models (section 2b). In our analysis, cyclone centers in reanalyses and model output are those identified objectively by TRACK, which ensures dynamical consistency between cyclone positions and the geopotential

height field. This differs from Bieli et al. (2020), who centered reanalysis geopotential data on best-track storm locations. The approach taken in our study avoids any potential inconsistencies between reanalysis and best-track storm centers, which would need to be accounted for, particularly at weaker intensities (Hodges et al. 2017).

Among existing studies, various phase-space thresholds have been employed to identify ET (e.g., Bieli et al. 2019; Hart and Evans 2001; Kofron et al. 2010; Liu et al. 2017; Zarzycki et al. 2017). We defined ET onset as either cold-core development (i.e., $T_L < 0$) or development of thermal asymmetry (i.e., $B \geq 10$), thereby allowing for either ET pathway. ET completion is defined as the first occurrence of both $B \geq 10$ m and $T_L < 0$. These thresholds are suitable for high-resolution gridded data (Michaelis and Lackmann 2019) and are supported by cluster analysis of observed ET events (Arnott et al. 2004). However, much of the ET identification literature has focused on the North Atlantic, yet ET phase-space pathways may differ between ocean basins (Bieli et al. 2019). To account for these difficulties in our global study, ET was identified only where the completion criterion is satisfied for at least four consecutive time steps (i.e., one day). The use of this additional one-day criterion identifies meaningful temporal changes in B and T_L and avoids counting any spurious, high-frequency temporal variability in phase-space parameters as multiple core-structure changes, following Baker et al. (2021). An analysis of the sensitivity of ET location to methodological choices is presented in section S1.2 in the online supplemental material, showing a large spread in ET location (Fig. S2). In this study, ET completion latitude was identified after a warm-core structure persisted for at least 2 days based on phase space parameters (i.e., $T_L > 0$ and $T_U > 0$), corresponding to w in Fig. S2. As such, sample sizes (Tables 1 and 3) remain unchanged. This method avoids false positives in ET identification arising from tropical depressions and other weak precursor systems (Bieli et al. 2020) and is therefore more appropriate to analysis of ET location (see section S1.2 in the online supplemental material for details).

e. Identifying post-ET reintensification

Instances of post-ET reintensification were defined as a post-ET change in p_{min} of at least -4 hPa, a threshold that is based on published case studies (e.g., Zhu et al. 2018), but the number of identified reintensification events is necessarily sensitive to this threshold. For consistency, we applied a single threshold across all reanalyses and models; a higher threshold will likely be appropriate for any future analysis of higher-resolution (i.e., convection-permitting) models. We used p_{min} to avoid any complications arising from intermodel differences in how near-surface wind speeds are computed (e.g., related to surface roughness).

f. Eady growth rate

Eady growth rate maxima [Eq. (4)] were computed as (Hoskins and Valdes 1990)

$$\sigma_{max} = 0.31 \frac{f}{N} \frac{\partial(u,v)}{\partial Z}, \tag{4}$$

where f is the Coriolis parameter, N is the static stability parameter, Z is geopotential height, and u and v are the zonal and meridional winds, respectively, which were used to compute the magnitude of the horizontal wind (i.e., $\sqrt{u^2 + v^2}$). The vertical derivatives, $\partial(u, v)$ and ∂Z, were computed between the 850- and 250-hPa levels using 6-hourly data.

3. Results

In each of the following sections, we present historical results and model evaluation followed by analysis of projected future changes out to 2050.

a. Spatial cyclone statistics

We first present spatial track density patterns for tropical cyclones undergoing ET in reanalyses and simulated across the PRIMAVERA ensemble. Reanalyses exhibit a high degree of consistency for track density and demonstrate that tropical cyclones undergo ET in all ocean basins. However, fewer ET events are identified over the northern Indian Ocean (Fig. 1a), where relatively low-latitude landfall either disrupts liminal ET events or averts potential ET cases altogether, primarily via boundary layer frictional effects (Bieli et al. 2019). Overall, basins' climatological ET activity is proportional to their tropical cyclone activity. The highest ET frequencies are identified in both the western North Pacific and South Pacific basins, with climatological mean values of ~12 cyclones per year. The North Atlantic is the most active basin for ET outside the Pacific, and comparably low activity occurs across the South Atlantic and south Indian basins (Fig. 1a).

The frequency of ET events simulated by PRIMAVERA models increases when resolution is increased from ~100 to ~25 km in all basins, both in the highresSST-present (Fig. 1b) and hist-1950 (Fig. 1d) experiments. Ensemble-mean climatologies are similar between both experiments (Fig. S3). The North Atlantic and western North Pacific basins are regions of relatively widespread intermodel agreement on the sign of this resolution-sensitivity in track density, again regardless of whether SST is prescribed. When prescribed, intermodel agreement is also identified in the South Pacific and south Indian basins (Fig. 1b). This result is consistent with a recent equivalent analysis of all tropical cyclones in PRIMAVERA simulations (Roberts et al. 2020a), where increased frequencies were simulated at higher model resolution across all ocean basins, for which the leading explanation is that finer atmospheric resolution increases the conversion rate of precursor vortices (or "seeds") to tropical cyclones (Roberts et al. 2020a; Vecchi et al. 2019; Vidale et al. 2021). Tropical cyclone intensities simulated at model resolutions in the range 50–20 km are more comparable with observational estimates (Roberts et al. 2020a), due in part to enhanced surface latent heat flux (Vannière et al. 2020), implying that a more realistic proportion may withstand midlatitude environmental conditions hostile to tropical cyclones prior to and during the initial stages of ET. At low resolutions (typically ~100 km), PRIMAVERA models simulate too few ET systems compared with reanalyses, particularly across the North Atlantic and western North Pacific, in both the highresSST-present (Fig. S4a) and hist-1950 (Fig. S4c) experiments. Increasing resolution to ~25 km leads to increased track density globally, reducing negative biases in these basins but engendering positive biases in the eastern North Pacific and South Pacific (Figs. S4c,d). In hist-1950, this bias reduction is consistent with a reduction in negative surface temperature biases at high resolution (e.g., ~1°K reduction in the North Atlantic; Moreno-Chamarro et al. 2022). In section 3b, we examine ET frequency and the percentage of tropical cyclones undergoing ET separately.

Overall, PRIMAVERA simulations indicate that increasing resolution improves the representation of ET frequency, as measured by track density, particularly across the North Atlantic and western North Pacific (Figs. 1c,e). For these basins, reductions in ensemble-mean absolute biases are found in both highresSST-present and hist-1950, and areas of bias reduction across multiple models occur primarily over western boundary currents—the Gulf Stream and Kuroshio, respectively. That these regions of resolution dependence and reduced biases overlap indicates that capturing the sharpness of SST fronts and associated baroclinicity is important in simulating ET (Evans et al. 2017; Klein et al. 2002); consistent with this, we find enhanced meridional SST gradients in both of these boundary current regions (Fig. S5). In the Southern Hemisphere, little difference in ensemble-mean biases is found between resolutions, with a caveat that observational or reanalysis-based climatologies for the Southern Ocean are themselves more uncertain (Hodges et al. 2017). The PRIMAVERA ensemble provides evidence that atmospheric resolutions typical of CMIP6 are too coarse to adequately capture basin-mean tropical cyclone (Roberts et al. 2020a) and ET statistics (this study). Increasing resolution to ~25 km partly addresses this shortcoming.

The climate change response of track density for tropical cyclones undergoing ET in high-resolution simulations is basin-dependent, with differences between atmosphere-only and fully coupled simulations also apparent. In highresSST-future, increased track density is simulated across the North and South Atlantic (but decreased over the eastern United States)
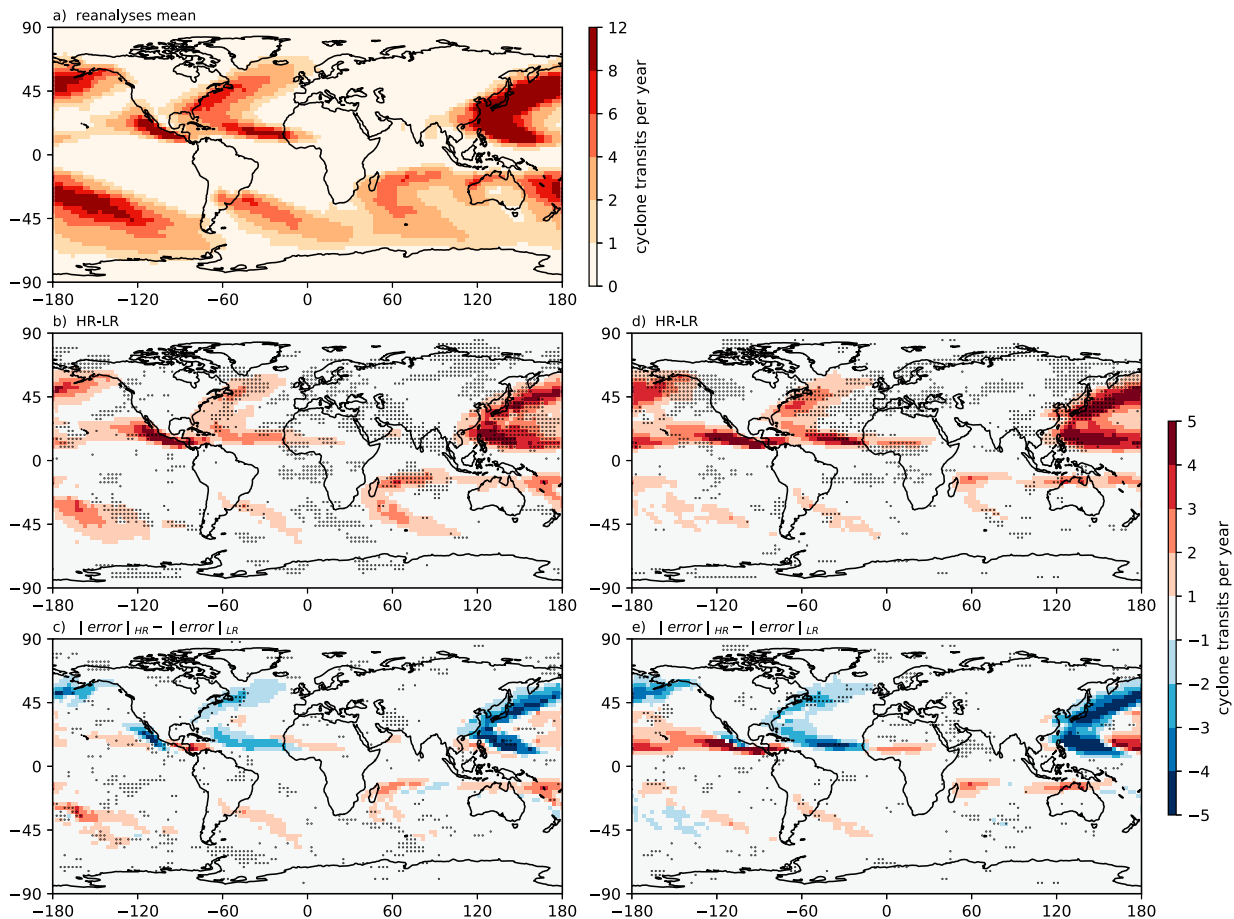
FIG. 1. Cyclone track density for all tropical cyclones undergoing ET. (a) Multi-reanalysis mean, (b),(c) highresSST-present, and (d),(e) hist-1950. Track density was computed from complete tracks, including precursor stages, and is shown in units of cyclone transits per year per unit area (within a 5° geodesic radius of storm centers). All available reanalysis years (Table 1) are included in this analysis. In (b) and (d) HR − LR denotes the ensemble-mean difference between high and low resolution. In (c) and (e) |error|$_{HR}$ − |error|$_{LR}$ denotes the ensemble-mean difference of the absolute error (model vs multi-reanalysis mean) between high and low resolution. The low-resolution (LR) subensemble includes CNRM-CM6.1-LR, EC-Earth3P-LR, ECMWF-IFS-LR, HadGEM3-GC3.1-LM(-LL), and MPI-ESM1.2-HR. The high-resolution (HR) subensemble includes CNRM-CM6.1-HR, EC-Earth3P-HR, ECMWF-IFS-HR, HadGEM3-GC3.1-HM(-HH), and MPI-ESM1.2-XR. In (b)–(e), stippling indicates where all five models agree on the sign of the difference.

and over the Maritime Continent; decreases are simulated over the eastern and western North Pacific and south Indian basins; and an unclear, mixed response characterizes the north Indian Ocean (Figs. 2a,b). Intermodel agreement about the sign of these changes is largely confined to cyclogenesis regions (e.g., equatorial West Africa) and over the Gulf Stream and Kuroshio. In highres-future simulations, positive climate change responses are confined to the central and eastern North Pacific. The spatial response pattern over the North Atlantic—increased over central and eastern North Atlantic and decreased along the United States' east coast—is similar between highresSST-future and highres-future, but the magnitude of the response is reduced in the fully coupled simulations (Figs. 2d–f). This spatial pattern is supported by recent projections, with increases particularly apparent in the eastern North Atlantic (Liu et al. 2017), consistent with the projected eastward and poleward

expansion of cyclogenesis within this basin (Haarsma et al. 2013).

Increasing horizontal resolution has a localized effect on the climate change response of track density for ET (Figs. 2c,f). In highresSST-future, resolution-sensitive responses to climate change, which are common across *all* models, are seen only over the central North Atlantic and parts of the Southern Ocean. In highres-future, spatially coherent and resolution-sensitive responses to climate change are seen over the South Atlantic and eastern North Pacific bains, where simulated track density maxima are shifted equatorward at high resolution. However, the spatial patterns of resolution sensitivity over the North Atlantic and western North Pacific broadly resemble the spatial climate change response patterns, which indicates that these responses are enhanced at high resolution in most models. This is seen more clearly in the atmosphere-only
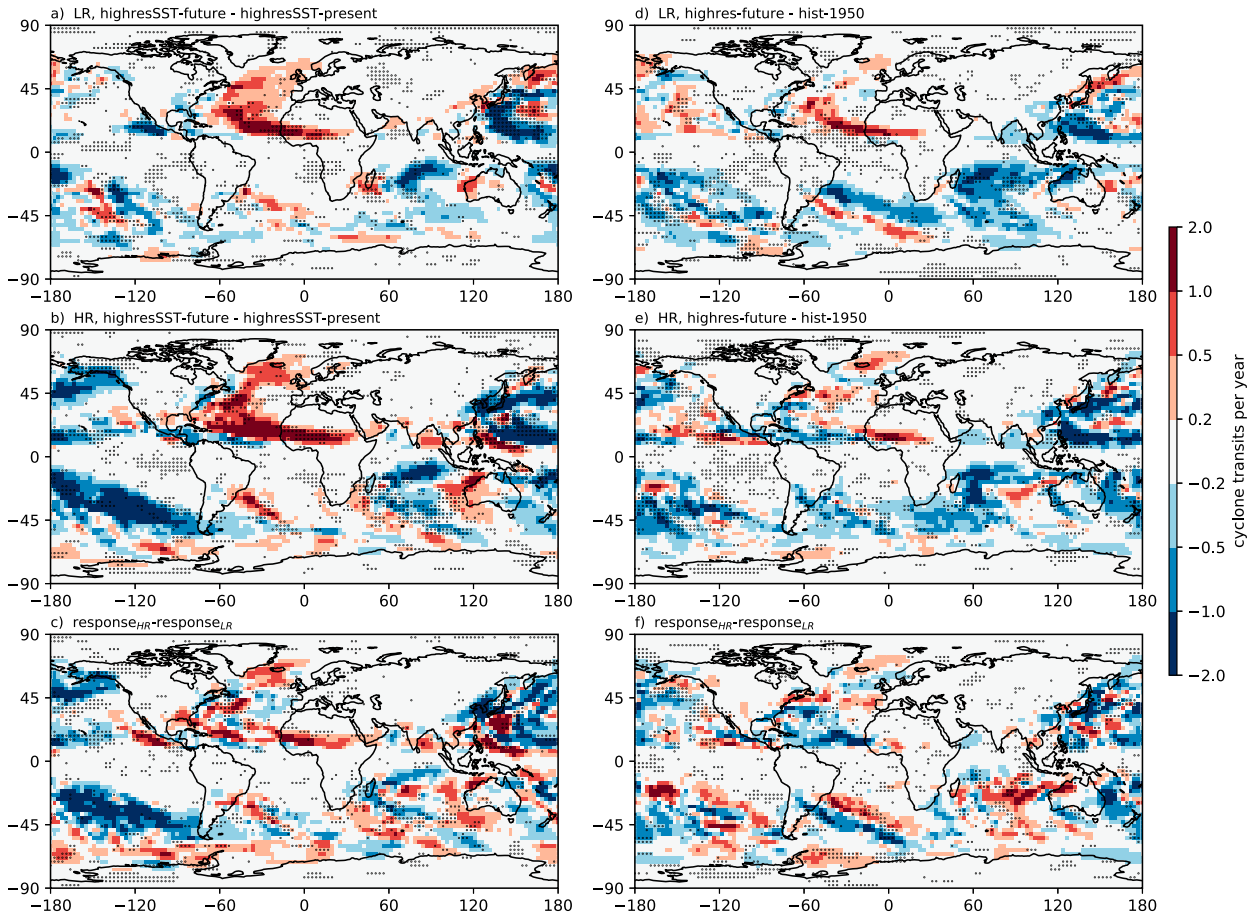
FIG. 2. Climate change response of track density for all cyclones undergoing ET: (a)–(c) highresSST-future minus highresSST-present and (d)–(f) highres-future minus hist-1950. Track density was computed from complete tracks, including precursor stages, and is shown in units of cyclone transits per year per unit area (within a 5° geodesic radius of storm centers). The low-resolution (LR) subensemble includes CNRM-CM6.1-LR, EC-Earth3P-LR, HadGEM3-GC3.1-LM(-LL), and MPI-ESM1.2-HR. The high-resolution (HR) subensemble includes CNRM-CM6.1-HR, EC-Earth3P-HR, HadGEM3-GC3.1-HM(-HH), and MPI-ESM1.2-XR. Stippling indicates where all models agree on the sign of the difference.

experiment (Fig. 2c) than in the fully coupled experiment (Fig. 2f).

b. Interannual variability in ET

Over the period 1979–2018, high-resolution highresSST-present simulations reproduce the multi-reanalysis-mean climatological ET counts for Northern Hemisphere basins (Fig. 3, left), except for the northern Indian Ocean, a basin where few ET events occur. However, little improvement with increased resolution is seen for Southern Hemisphere basins (Fig. 3, left). Again, uncertainty is higher across the Southern Ocean, with greater inter-reanalysis spread seen for Southern Hemisphere basins. These results are also true of the hist-1950 simulations (Fig. 4, left). The highresSST-present simulations appear to capture decadal variability in the role of SST in sustaining tropical cyclones to ET. In certain basins, periods are apparent where the highresSST-present ensemble mean and multi-reanalysis mean ET count match well, such as 1985–2000 for the North Atlantic and 1990–2005 for the western North Pacific (Fig. 3, left). These periods coincide

with observed positive phases in Atlantic multidecadal variability and Pacific decadal oscillation, respectively. For ET percent, differences between low- and high-resolution ensemble means are small for most basins (Fig. 3, right). This suggests that the large-scale environmental conditions conducive to ET are not substantially different across the range of model resolutions considered here. This indicates that increased ET frequency at high resolution is driven primarily by increased tropical cyclone frequency, not by an increase in ET percent. Similar mean values and variance in ensemble-mean ET count and ET percent are simulated in both highresSST-present (Fig. 3) and hist-1950 (Fig. 4) experiments.

In highresSST-present, models' skill in reproducing the multi-reanalysis-mean interannual variability in ET count varies between basins (Table 4). Interannual variability in ensemble-mean and multi-reanalysis-mean ET counts are significantly, positively correlated for three basins at low resolution and four basins at high resolution. The North Atlantic and western North Pacific basins are significantly correlated
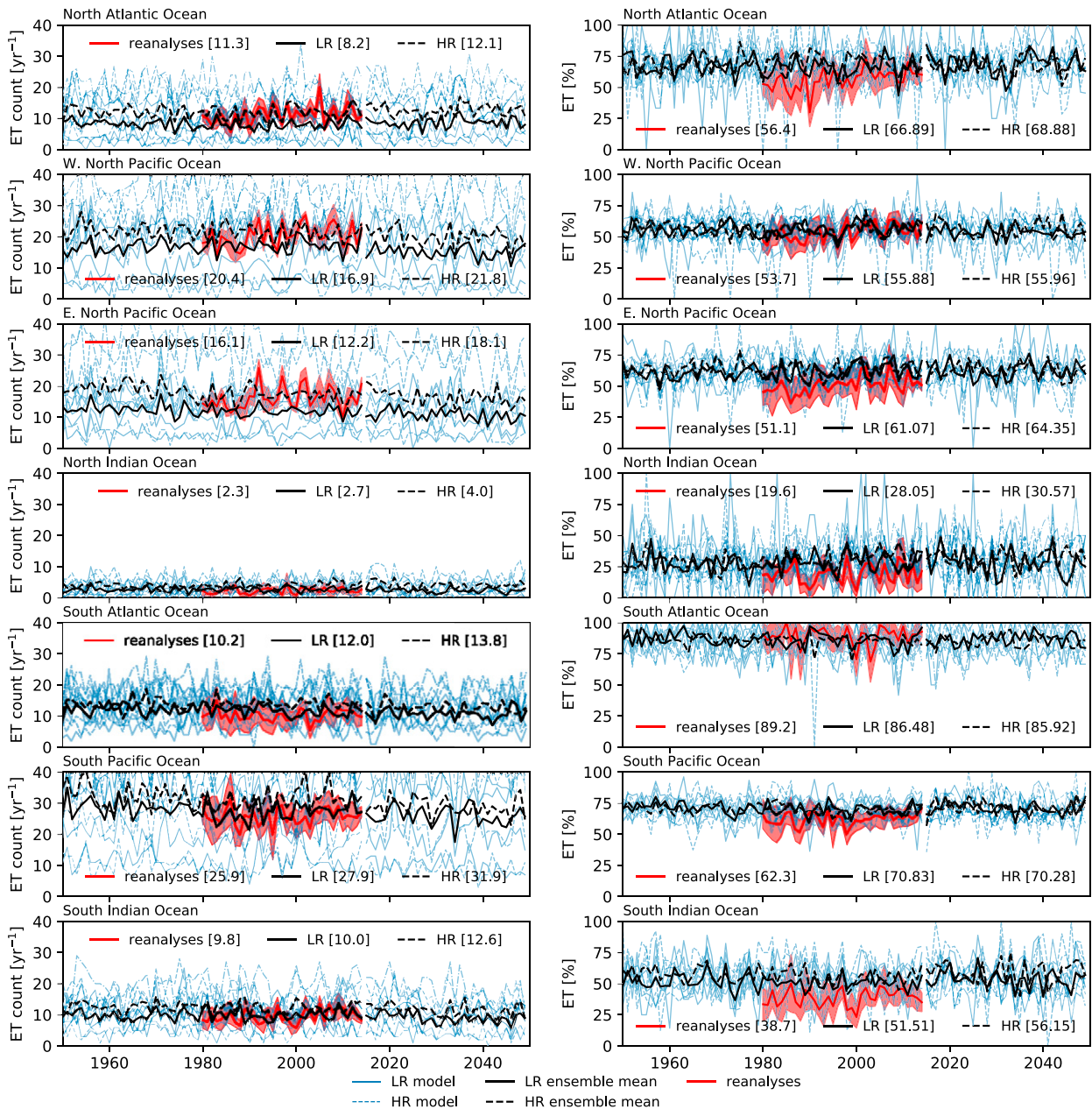
FIG. 3. Interannual variability in (left) the number of ET events and (right) the percentage of tropical cyclones undergoing ET in each ocean basin in reanalyses and simulated in highresSST-present and highresSST-future experiments. Shown are (red) the multi-reanalysis mean, with one standard deviation of the reanalysis spread indicated by red shading, and low- (solid black) and high-resolution (dashed black) ensemble means. Each panel's legend gives climatological-mean values of (left) ET count or (right) ET percent for the reanalyses and historical simulations. Also shown are (blue) time series for individual simulations to indicate the ensemble spread for each basin.

at both resolutions; the South Atlantic and South Pacific basins are significantly correlated only at high resolution; and the eastern North Pacific is significant only at low resolution. Only for the north and south Indian basins is ensemble-mean variability uncorrelated with reanalyses at either resolution. (Correlation coefficients for hist-1950 simulations are not shown because it is not expected that fully coupled models' internal year-to-year variability would mimic that of forced simulations

or reanalyses.) For ET percent, fewer significant correlations are found between ensemble-mean and multi-reanalysis-mean time series (Table 4). Positive correlations are seen in the northern and southern Indian basins and in the South Pacific basin at high resolution. However, low- and high-resolution ensemble-mean ET percent time series covary in most basins in both highresSST-present (Fig. 3) and hist-1950 (Fig. 4), more so than for ET count. To explain this, we hypothesize
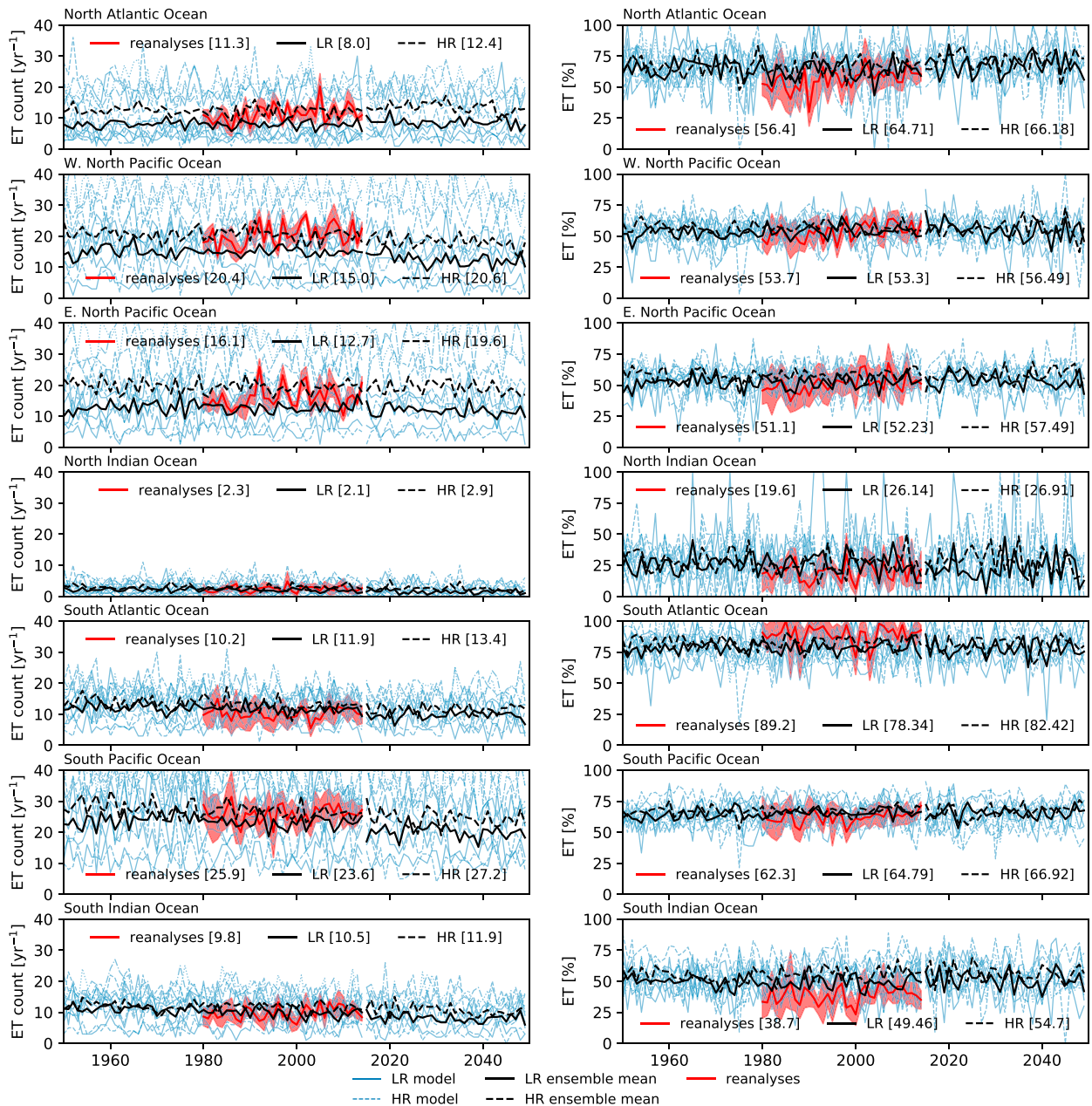
FIG. 4. As in Fig. 3 for fully coupled hist-1950 and highres-future simulations.

that the large-scale environment conducive to the baroclinic conversion of tropical cyclones is less sensitive to model resolution, while ET count depends on tropical cyclone count, which is sensitive to model resolution (Roberts et al. 2020a).

Recent analysis of an ensemble of HadGEM3-GC3.1 simulations, performed under HighResMIP, demonstrated that mean skill in representing interannual variability in tropical cyclone count improves with additional members (Roberts et al. 2020a). At present, the required 6-hourly geopotential outputs are available for too few ensemble members to repeat such an analysis for tropical cyclones undergoing ET, but this would constitute valuable future work when sufficient model

output is obtainable. Nonetheless, quantifying the level of skill that exists in capturing interannual variability in the subset of tropical cyclones that undergo ET, while lower than that for all tropical cyclones, is important, establishing the baseline for HighResMIP-class models. This prompts further examination of ET seasonality in the historical and future atmosphere-only simulations, which is possible in the continuous PRIMAVERA simulations.

c. Historical and future ET seasonality

We next evaluate the seasonal cycle of ET, focusing on the North Atlantic and western North Pacific basins for which

TABLE 4. Pearson's *r* coefficients for correlations between low- (LR) or high-resolution (HR) ensemble-mean and multi-reanalysis-mean interannual variability in ET count and ET percent for each ocean basin. Coefficients are shown only for highresSST-present; hist-1950 simulations are not shown because it is not expected that coupled models' internal year-to-year variability would mimic that of forced simulations or reanalyses. Significant ($p < 0.1$) correlations are in bold type.

	ET count		ET percent (%)	
Ocean basin	LR	HR	LR	HR
North Atlantic	**0.31**	**0.30**	0.24	−0.16
Western North Pacific	**0.50**	**0.34**	0.21	0.24
Eastern North Pacific	**0.43**	0.22	**0.42**	0.16
North Indian	−0.08	0.03	0.03	**0.38**
South Atlantic	0.07	**0.34**	0.12	0.27
South Pacific	0.08	**0.50**	0.17	**0.34**
South Indian	−0.04	−0.19	0.24	**0.33**

both climatological ET statistics (Fig. 1) and interannual ET variability (Table 4) are represented reasonably across models. In the North Atlantic, reanalyses show ET percent increasing from July to a peak in September before declining into winter (Fig. S6a). In the highresSST-present experiment, most models reproduce this seasonality, but the magnitude of the seasonal peak is overestimated by ~10% at high resolution. There are indications that increased atmospheric resolution improves the simulation of the timing of the seasonal ET percent peak. Two models—CNRM-CM6.1 and EC-Earth3P—simulate the seasonal peak too early (in August) at low resolution but simulate a later peak (in September) at high resolution. Additionally, MPI-ESM1.2, the lowest-resolution model in this ensemble, simulates comparably muted seasonality that also peaks earlier than reanalyses at both resolutions. In the fully coupled hist-1950 experiment, models reproduce the multi-reanalysis-mean seasonal cycle, but HadGEM3-GC3.1 and CNRM-CM6.1 simulate a broader seasonal distribution compared with reanalyses (Fig. S7a). In the western North Pacific, reanalyses show bimodal seasonality, with peaks in ET percent in May and September (Fig. S6b). Excepting the MPI-ESM1.2 model, which does not capture bimodality, highresSST-present simulations also exhibit two seasonal peaks, but each occurs one to two months later than in reanalyses in both low- and high-resolution integrations (Fig. S6b), and this also holds true for hist-1950 simulations (Fig. S7b).

To assess any potential future change in seasonality, ΔET percent, we differenced the historical and future seasonal cycles. For the North Atlantic, despite pronounced intermodel spread throughout most of the annual cycle, there is an indication of more consistent model behavior during August–November, months for which most models simulate an increase in ET percent in both the highresSST-future (Fig. S6c) and highres-future experiments (Fig. S7c). To quantify the degree to which this intermodel consistency represents secular change in ET seasonality, the annual fraction of total annual ET events occurring during August–November was computed. A significant, positive trend in this quantity over the period 1950–2050 is found in the
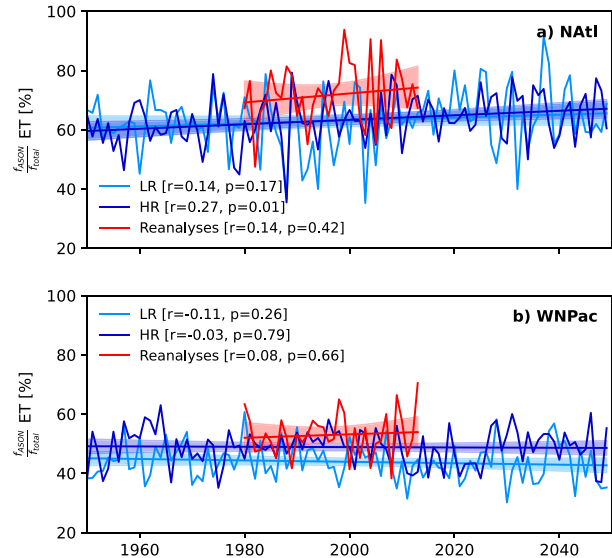

FIG. 5. Secular change in the proportion of ET events occurring during August–November in reanalyses (red) and low- (pale blue) and high-resolution (dark blue) atmosphere-only simulations (ensemble mean) for the (a) North Atlantic and (b) western North Pacific basins. Shading shows the 95% confidence interval for the linear fit. ECMWF-IFS is not included in this analysis because no future simulations were performed in HighResMIP for this model.

ensemble mean of high-resolution atmosphere-only simulations (Fig. 5a), but the trend is not significant in reanalyses, which likely cover too short a period (1980–) to assess secular change, and is significant in the low-resolution ensemble mean only at the 80% level. In fully coupled simulations, no significant trends are seen (Fig. S8a). Conducting a similar analysis of the forthcoming extension of ERA5 back to 1950 is warranted, presatellite observational uncertainty notwithstanding. For the western North Pacific, the intermodel spread during the annual cycle of ΔET percent is similar between highresSST-future (Fig. S6d) and highres-future simulations (Fig. S7d) and, in contrast to the North Atlantic, no significant secular change in ET seasonality is found in either reanalyses or in PRIMAVERA simulations out to 2050 (Fig. 5b; see also Fig. S8b). However, together with projected changes in track density (Figs. 2a,b,d,e), these results provide further evidence that the future response of ET to climate change across the North Atlantic differs from that of the western North Pacific and of other ocean basins. Therefore, we next investigate the role of cyclone structure in explaining these distinct North Atlantic and western North Pacific responses.

d. Response of cyclone structures to climate change

To examine the response of cyclone core structure to climate change, we computed ensemble-mean bivariate frequency distributions of phase-space parameters, B, T_L, and T_U in the high-resolution simulations. The $T_L - B$ distribution exhibits a similar general structure in the highresSST-present and highresSST-future experiments for both the North Atlantic (Figs. 6a,b) and western North Pacific (Figs. 6d,e) basins. This is also true
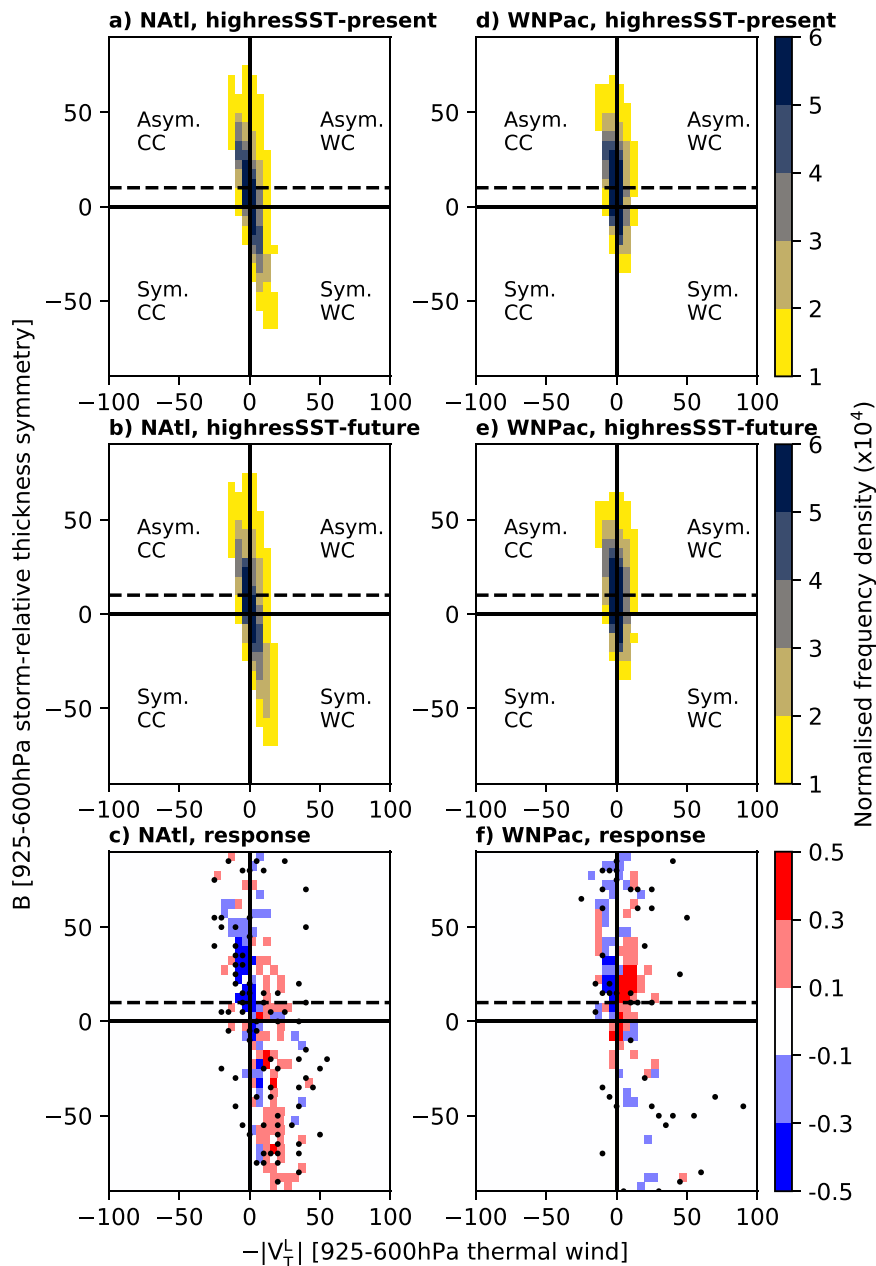
FIG. 6. Ensemble-mean distributions of T_L vs B in high-resolution (a),(d) highresSST-present and (b),(e) highresSST-future simulations, as well as (c),(f) the climate change response for the North Atlantic (NAtl) and western North Pacific (WNPac). Distributions are computed from every 6-hourly point during the entire lifetime of all storms undergoing ET, plotted as two-dimensional histograms, and normalized by the total number of cyclones (sample sizes for each model are given in Table 3). Values are scaled by 10^4. Cyclone phase-space categories are warm-core (WC) or cold-core (CC) and either symmetrical (Sym; i.e., nonfrontal) or asymmetrical (Asym; i.e., frontal). The threshold of 10 m used to distinguish thermally symmetric from asymmetric cyclones is indicated (dashed line). Stippling in (c) and (f) indicates where all models agree on the sign of the difference.

for $T_L - T_U$ distributions (Figs. 7a,b,d,e). Generally, tropical cyclones undergoing ET occupy the lower-right (symmetric, warm core) and upper-left (asymmetric, cold core) quadrants, with fewer instances in either hybrid (transitional) quadrant. The phase-space parameter distributions simulated across

PRIMAVERA models are consistent with previous studies (Hart et al. 2006; Michaelis and Lackmann 2019). Historical ensemble-mean values of B and T_L for the North Atlantic are consistent with recent analysis of observations (Studholme et al. 2015) as well as reanalyses and Community Atmosphere
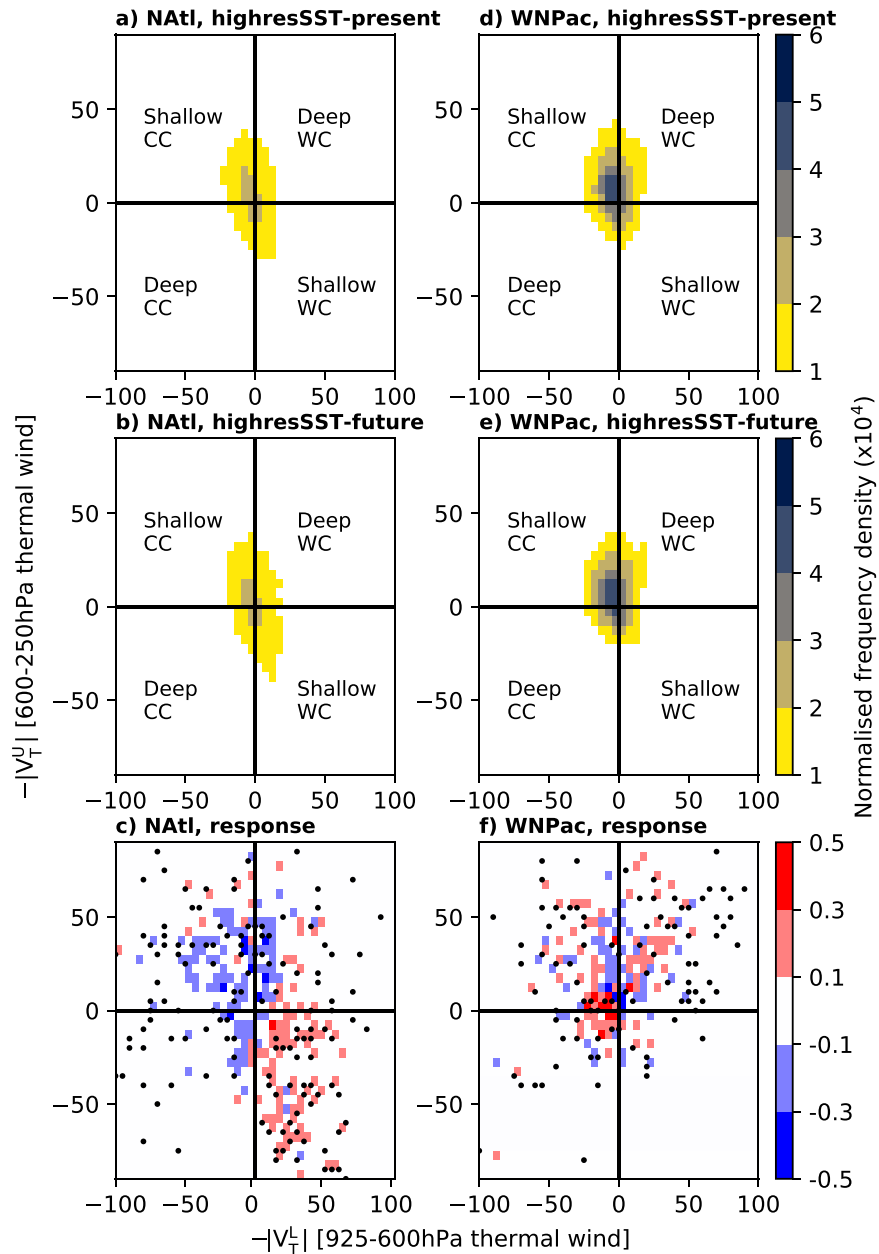
FIG. 7. Ensemble-mean distributions of T_L vs T_U in high-resolution (a),(d) highresSST-present and (b),(e) highresSST-future simulations, as well as (c),(f) the climate change response for the North Atlantic (NAtl) and western North Pacific (WNPac). Distributions are computed from every 6-hourly point during the entire lifetime of all storms undergoing ET, plotted as two-dimensional histograms, and normalized by the total number of cyclones (sample sizes for each model are given in Table 3). Values are scaled by 10^4. Cyclone phase-space categories are shallow or deep warm- (WC) or cold-core (CC). Stippling in (c) and (f) indicates where all models agree on the sign of the difference.

Model simulations at resolutions of 55 and 28 km (Zarzycki et al. 2017). Ensemble-mean T_U values are also consistent with these existing studies, except that deep warm-core structures are less frequent in PRIMAVERA models than in recent 15-km-resolution simulations with the Model for Prediction Across Scales–Atmosphere model (Michaelis and Lackmann 2019), likely due to differences in atmospheric resolution. For the western North Pacific, model-simulated phase-space parameters are consistent with reanalysis-based values (Kitabatake 2011). In the fully coupled simulations, $T_L - B$ distributions for

both basins are similar to those of the atmosphere-only simulations (Figs. 8c,f), but differences in ensemble-mean T_U values are seen, with warm-core responses to climate change occurring variously throughout the troposphere (Figs. 9c,f).

Under climate change, models forced by prescribed SST simulate stronger warm-core structures in the North Atlantic, indicated by a shift toward higher T_L for axisymmetric tropical cyclones (Fig. 6c). Moreover, $T_L - T_U$ distributions show that the future shift to stronger warm-core structures is primarily confined to the lower troposphere (Figs. 7c,f). (Here, "strong" refers to ensemble-mean T_L values at the higher end of the historical distributions, in which a range of model-simulated intensities are averaged.) These findings are supported by a recent single-model study (Michaelis and Lackmann 2019), albeit the ensemble-mean signal we report is less pronounced, and are consistent with increased low-level moisture and the potential for enhanced latent heat release in a warmer climate. Future changes in core structures offer a partly mechanistic explanation of the projected increase in ET across the North Atlantic (Baatsen et al. 2015; Haarsma et al. 2013; Liu et al. 2017) as well as the projected change in track density, which is largely unique to the North Atlantic (Figs. 2a,b,d,e). The lesser energy of weak warm-core cyclones is more likely to dissipate before ET may occur, but relatively strong warm-core structures make cyclones more resilient to unfavorable midlatitude environmental conditions (primarily cooler SST and increased vertical wind shear), prolonging their poleward propagation and making ET more probable across the North Atlantic (Hart et al. 2006).

In the North Pacific, however, this future shift to stronger warm cores is not seen in PRIMAVERA models (Fig. 6f), although more frequent asymmetric, warm-core hybrid structures (upper-right quadrant) in the future are simulated. These instances of hybrid structures show cyclones existing more frequently in the transitional quadrants, potentially indicating a future elongation of ET time (Zarzycki et al. 2017) and an increase in warm-seclusion occurrences, which involve multiple transitions (Baker et al. 2021; Dekker et al. 2018). Also seen is a shift toward stronger upper-level, cold-core structures (Fig. 7f). The western North Pacific is therefore characterized by more mixed future changes in core-structure frequencies, consistent with the projected response of track density, which generally decreases across the basin but increases in localized areas (Figs. 2b,e). Broadly, these results are also consistent with the lack of any consensus in published projections of ET frequency across the western North Pacific: both a less favorable future ET environment (Ito et al. 2016) versus moderate future increase in ET frequency (Bieli et al. 2020) have been suggested. For both basins, future phase-space changes in the fully coupled simulations resemble those seen in the atmosphere-only experiments, but the North Atlantic climate change signal is comparably muted (Figs. 8c,f and 9c,f).

Overall, these results help clarify the potential role that the climate change response of cyclones' core structures have in determining future ET frequency changes, and quantifies how this differs between basins. Differences in pre-ET structures potentially underpin basin-specific responses of ET to climate

change, and consistency exists among PRIMAVERA models. However, to fully explain what drives disparate North Atlantic and western North Pacific responses, further studies of future changes in cyclogenesis and midlatitude large-scale conditions are needed, based on models of higher resolution than those in PRIMAVERA, which better simulate the most intense systems (Judt et al. 2021), and, potentially, their interactions with the large-scale environment.

e. Pre- and post-ET cyclone intensity

During ET, cyclones develop low-level frontal structures and their horizontal size increases (Evans et al. 2017). As such, increasing model resolution is expected to impact the simulation of cyclones pre- and post-ET differently, particularly in models whose effective resolutions coarsen equatorward. However, performing a global analysis of the pre- and post-ET stages of tropical cyclones' life cycles is not trivial because ET pathways (i.e., the order in which B and T_L changes occur) differ between ocean basins (Bieli et al. 2019). We therefore separated cyclone tracks' warm- and cold-core stages about ET completion, when both B and T_L satisfy ET criteria, following the definition first used by Hart (2003). Our additional 1-day criterion (see section 2) helps increase confidence in the following intermodel comparison.

Compared with best-track intensity estimates, certain atmosphere-only models (particularly CNRM-CM6.1) simulate realistic intensities at resolutions in the range 20–50 km (Roberts et al. 2020a). However, best-track intensity estimates are not well suited to evaluating post-ET systems (Velden et al. 2006), and the available primary cyclone wind speed observations, such as satellite scatterometry data, seldom include cyclones' post-tropical stages and span too short a temporal range for climatological evaluation. We therefore turn to reanalyses, which are constrained by observational data, to provide a homogeneous global reference. An important caveat, however, is the underestimation of cyclone wind speeds in reanalyses (Hodges et al. 2017; Murakami 2014), although this underestimation is less marked at higher latitudes (Sainsbury et al. 2020).

Considering all storms globally, PRIMAVERA models reproduce the reanalyses' cold-core, post-ET intensity distributions at both low and high resolution and in both atmosphere-only and fully coupled simulations (Figs. 10 and 11, top rows). However, models' representation of warm-core, pre-ET distributions improve markedly with increasing resolution, especially for CNRM-CM6.1 and HadGEM3-GC3.1, but more clearly so in the atmosphere-only than in the fully coupled simulations, wherein cold-wake feedbacks reduce upper-ocean temperatures and weaken subsequent tropical cyclones (Balaguru et al. 2014). Sensitivity to resolution is similar in the fully coupled CNRM-CM6.1 and HadGEM3-GC3.1 simulations (Fig. 11, top row). These results show that horizontal resolutions typical of CMIP6 appear sufficient to simulate cold-core (post-ET) intensity distributions, including the relatively high-intensity tail—resolutions at which large-ensemble studies to quantify multiannual variability of the strongest post-ET storms are computationally feasible. However, among high-resolution PRIMAVERA models,
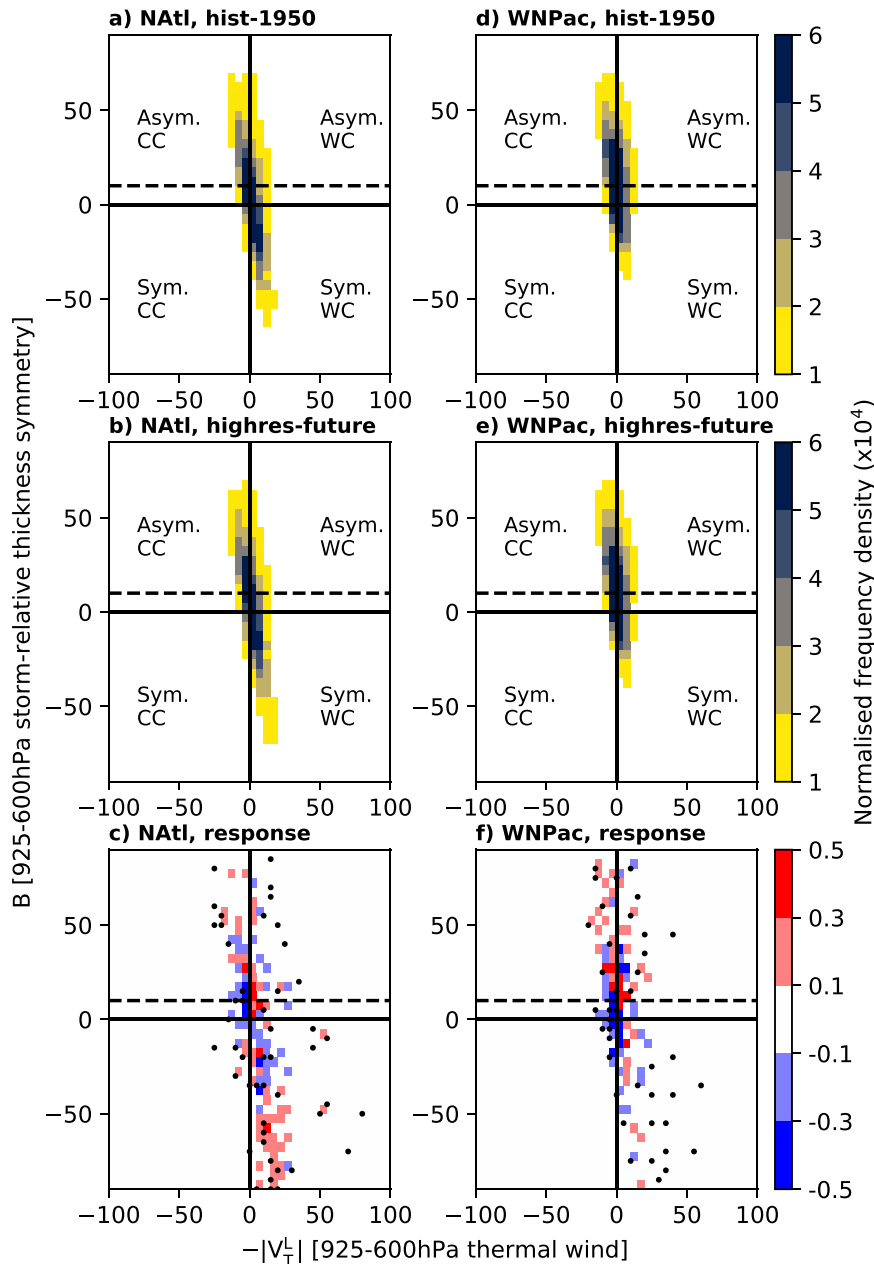
FIG. 8. As in Fig. 6, but for hist-1950 and highres-future experiments.

the high-intensity tail of the warm-core distribution is reproduced only by CNRM-CM6.1.

For highresSST-future, several models project decreasing warm-core and increasing cold-core intensities for weaker storms (<17 m s^{-1}) but simulate opposite warm- and cold-core responses for stronger storms (≥ 17 m s^{-1}) (Fig. 10, bottom row). This warm-core response is consistent with projections of intensified tropical cyclones under anthropogenic warming (Knutson et al. 2020). However, these responses are not replicated by fully coupled models (Fig. 11, bottom row), in which intensity changes are weak (Roberts et al. 2020b). In the fully

coupled simulations, the responses of pre- and post-ET intensity distributions to climate change are equivocal, with substantial intermodel differences. We speculate that the climate change forcing out to 2050 in the HighResMIP experimental protocol is insufficiently strong (i.e., the future simulation period is too short) for a clear signal to emerge. However, it is unclear whether intensity changes would be seen. For tropical cyclones overall, Roberts et al. (2020b) found a weak future intensification in these simulations, and Bieli et al. (2020) found equivocal ET climate change responses in many basins out to 2100 under the weaker RCP4.5 scenario. If a clear climate change signal
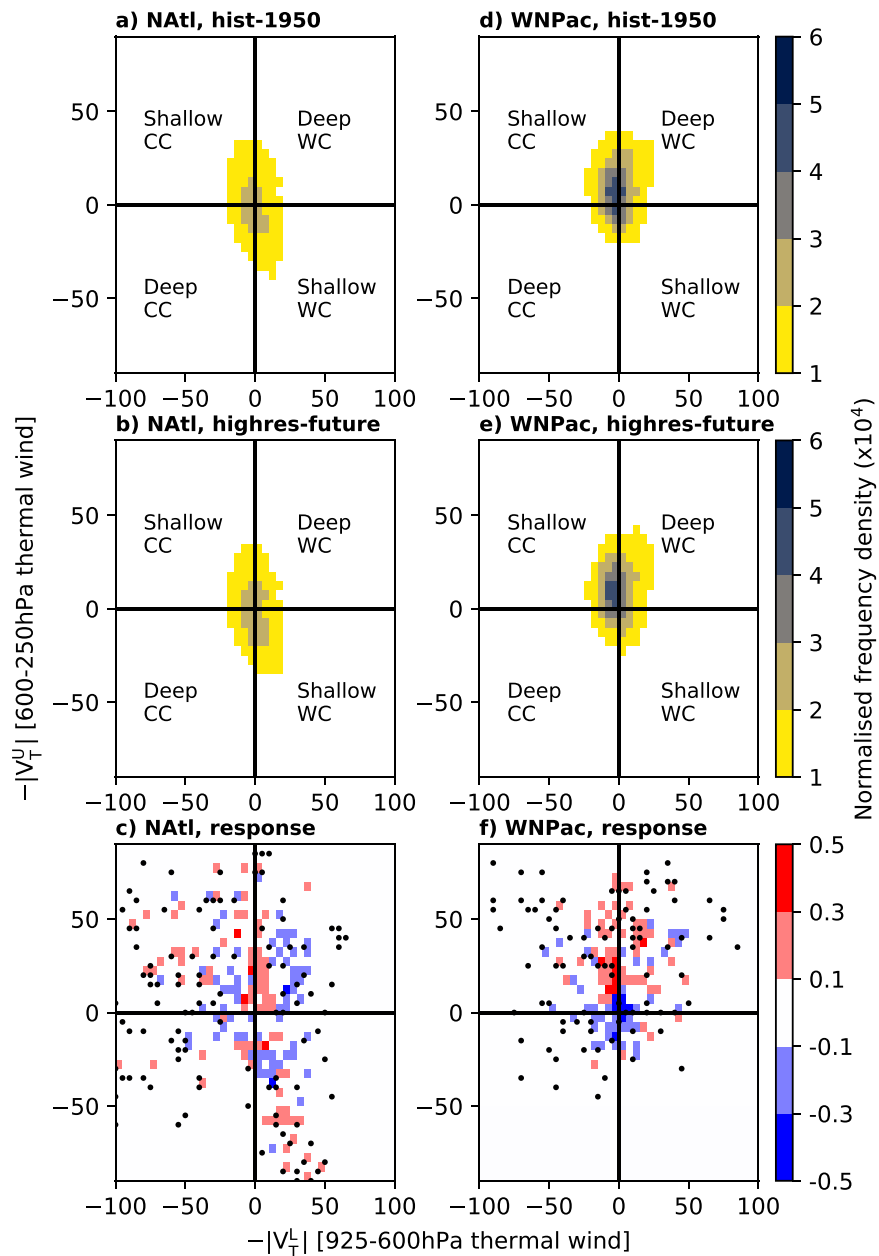
FIG. 9. As in Fig. 7, but for hist-1950 and highres-future experiments.

were to emerge with further increases in model resolution, which would increase the relative difference between the weakest and strongest simulated tropical cyclones, this would suggest that processes important for intensity change are not adequately captured at ~25-km resolution.

f. Post-ET reintensification

The lifetime maximum intensity of transitioning tropical cyclones typically occurs during the warm-core, tropical phase. However, the addition of a baroclinic energy source and cyclone–wave interactions induce post-ET reintensification (Evans et al. 2017). We quantified the frequencies of reintensifying versus nonreintensifying

cyclones in reanalyses and in the PRIMAVERA ensemble. Globally, reanalyses indicate that approximately 50% of tropical cyclones that complete ET undergo post-ET reintensification (Fig. 12a). For the North Atlantic and western North Pacific basins, ~55% and ~45%, respectively, reintensify (not shown), consistent with Hart and Evans (2001). These results are not significantly different when reintensification is defined using 925-hPa wind speed (not shown). Globally, PRIMAVERA models generally overestimate climatological reintensification frequency at low resolution, but increasing resolution decreases the proportion of reintensifying systems (and increases the proportion of nonreintensifying systems) in all models except MPI-ESM1.2,
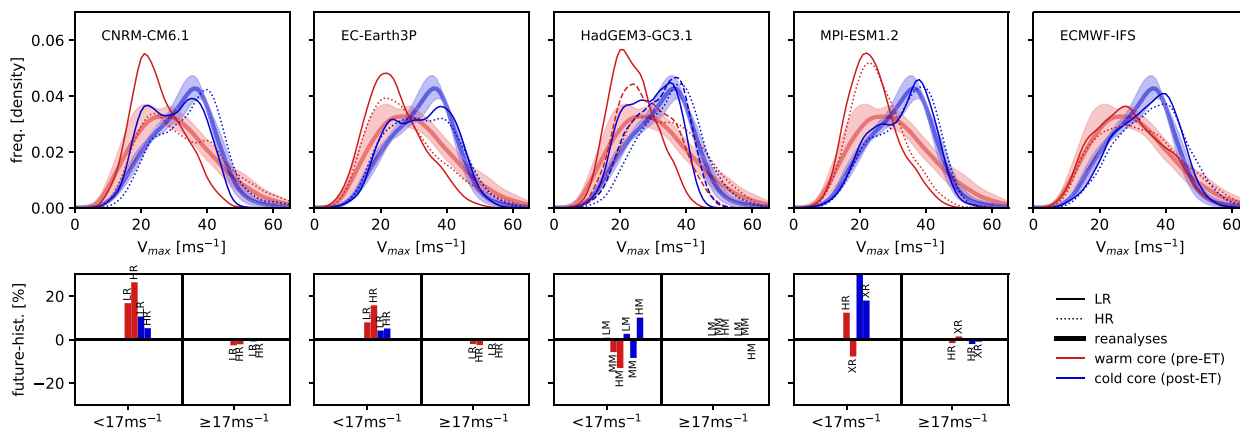
FIG. 10. Intensity (v_{max} at 925 hPa) distributions in atmosphere-only simulations for all cyclones undergoing ET globally. For each model, historical simulations are shown in the top row and future simulations in the bottom row. Multi-reanalysis-mean curves (thick solid lines) are shown with one standard deviation (shading). Both low- (thin solid lines) and high-resolution (thin dashed lines) simulations are shown. Climate change responses (i.e., highresSST-future minus highresSST-present), computed as integrated differences, are shown as percentages for storms whose lifetime maximum intensity is <17 m s^{-1} or ≥ 17 m s^{-1} for each atmospheric model resolution (ordered left to right).

which better matches reanalyses (Figs. 12b and 13b). This result potentially reflects improved simulation of the interactions between cyclones and the large-scale circulation, which acts to reintensify systems (Keller et al. 2019), at high resolution. Which processes facilitate such improvement should be a focus of future research because these processes will be important for risk assessments of reintensification. However, it is also possible that post-ET reintensification arises in models whose effective resolution increases with increasing latitude (e.g., HadGEM3-GC3.1), allowing stronger simulated winds at higher latitudes, but the impact of this artifact will be reduced at higher resolutions.

In HadGEM3-GC3.1, for an atmospheric resolution of 25 km (at 50° latitude), increasing ocean resolution from 1/4° to 1/12° (-HM and -HH, respectively) does not impact the proportion of reintensifying cyclones (Fig. 13b). An increase in the proportion might be expected because increasing ocean resolution and therefore more sharply resolving SST fronts (around western

boundary currents; Fig. S5) is likely to enhance baroclinicity and provide atmospheric conditions conducive to post-ET reintensification. That no increase is seen implies that atmospheric resolution, to which simulated tropical cyclone frequency and intensity are sensitive, acts as a constraint on reintensification statistics, at least for this particular model. Further investigation with multiple ocean models would establish more robustly whether this is the case.

In both the atmosphere-only and fully coupled simulations, future changes in the proportion of post-ET reintensifying systems are small and generally within one standard deviation of historical interannual variability (Figs. 12c and 13c), again suggesting that any climate change response under RCP8.5 emerges after 2050. In atmosphere-only simulations, low-resolution models all simulate an increase the proportion of reintensifying cyclones, but high-resolution models simulate a decrease (Fig. 12c), except for CNRM-CM6.1. Fully coupled models typically simulate a future increase across resolutions (Fig. 13c).
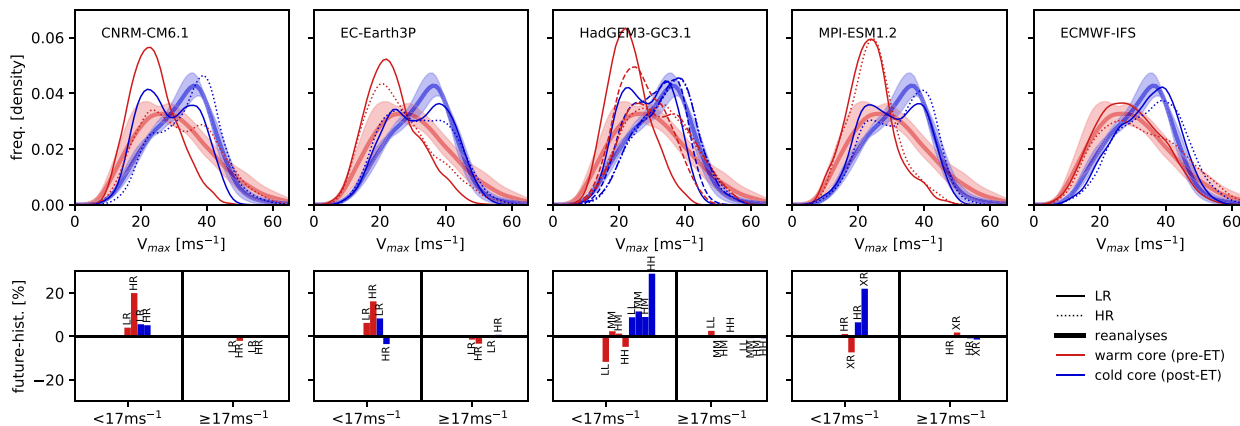

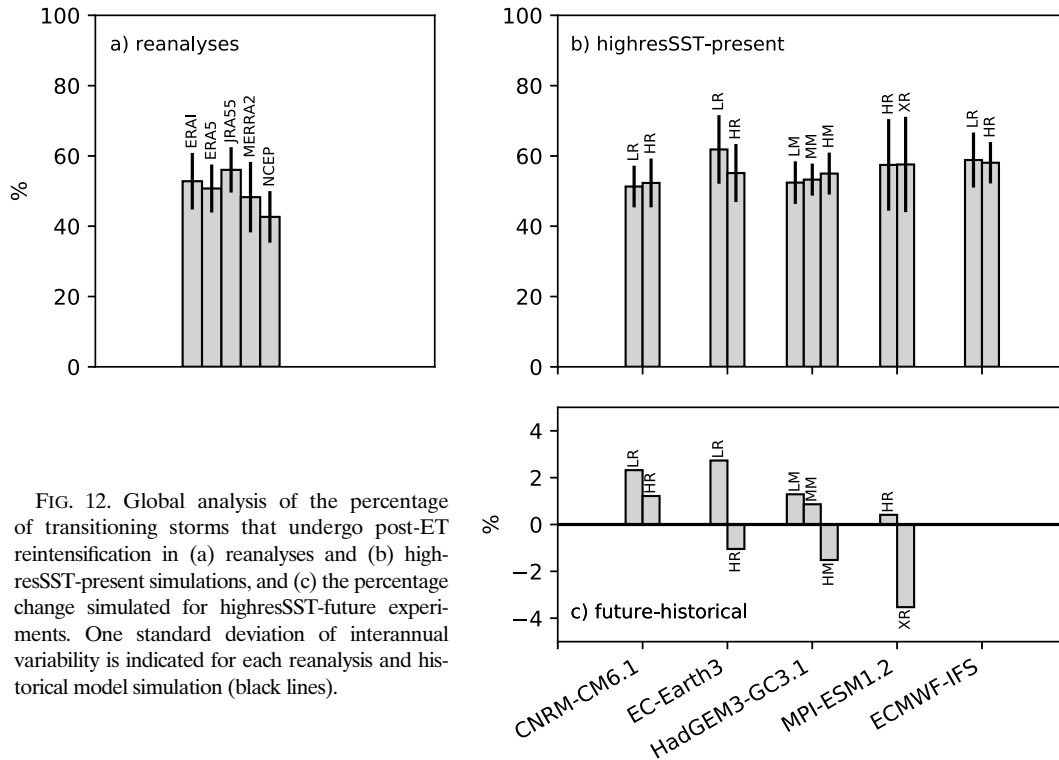FIG. 11. As in Fig. 10, but for fully coupled simulations.

FIG. 12. Global analysis of the percentage of transitioning storms that undergo post-ET reintensification in (a) reanalyses and (b) highresSST-present simulations, and (c) the percentage change simulated for highresSST-future experiments. One standard deviation of interannual variability is indicated for each reanalysis and historical model simulation (black lines).

g. ET latitude

Finally, we assess how ET location responds both to increased resolution and to climate change out to 2050. Distributions of ET-completion latitude were computed from reanalyses and all PRIMAVERA experiments globally as well as well as separately for the basins where models exhibit the best performance: the North Atlantic and western North Pacific basins (Fig. 14). For highresSST-present, model-simulated ET completion occurs at lower latitudes than in reanalyses (Figs. 14a–c). At high resolution, this is partially rectified: peak frequency occurs at a similar latitude to reanalyses in both the North Atlantic (Fig. 14a) and western North Pacific (Fig. 14b), but the magnitudes of both peaks are underestimated and occurrences of low-latitude ET (i.e., 10°–20°) remain too frequent. Globally, an equatorward bias in peak frequency across resolutions indicates that ET-completion latitude is less well simulated in other basins (Fig. 14c). These results hold true for hist-1950 simulations (Figs. 14d–f), except there are fewer instances of low-latitude ET (i.e., 10°–20°), likely reflecting slower development of warm-core structures and subsequent ET in the fully coupled experiments.

In response to climate change, the ensemble-mean distribution of ET completion latitude exhibits an equatorward shift in the North Atlantic in the atmosphere-only experiment (Fig. 14a), but a poleward shift in the fully coupled simulations (Fig. 14d), with an increased frequency of ET completion particularly between 45° and 55°N. In the western North Pacific, a poleward shift is seen in the latitude of the peak frequency, from ~30° to ~40°N, in both experiments, but little change is simulated at higher latitudes (i.e., >45°N). Globally, a small equatorward shift

of ~2° is simulated in atmosphere-only simulations (Fig. 14c) and no meridional shift is seen in coupled simulations (Fig. 14f). Previously, we showed stronger low-level warm-core structures are simulated in the future (Figs. 6 and 8), which potentially allows tropical cyclones to propagate farther poleward prior to ET, with the most pronounced signal seen in the North Atlantic. While coupled PRIMAVERA models provide evidence for a poleward shift of ET, climate change responses globally are equivocal out to 2050.

4. Summary and discussion

This paper presents an analysis of ET across five reanalysis datasets and climate simulations performed with five atmosphere-only and full coupled global models participating in CMIP6 HighResMIP, focusing on 1) the effect of increased model resolution on the representation of ET and 2) the response of ET to climate change.

For all tropical cyclones undergoing ET, we find an increase in the climatological track density simulated at high resolution (~25 km) compared with low resolution (~100 km) in all ocean basins and in both atmosphere-only and fully coupled model configurations (Figs. 1b,d), particularly over Northern Hemisphere western boundary currents. Model error in simulated track density (compared with the multi-reanalysis-mean track density) is reduced at high resolution in the North Atlantic and western North Pacific (Figs. 1c,e). The simulated climatological annual-mean count of ET events is closer to that of reanalyses in the ocean basins where ET activity is highest—the North Atlantic and the western and eastern North Pacific—in
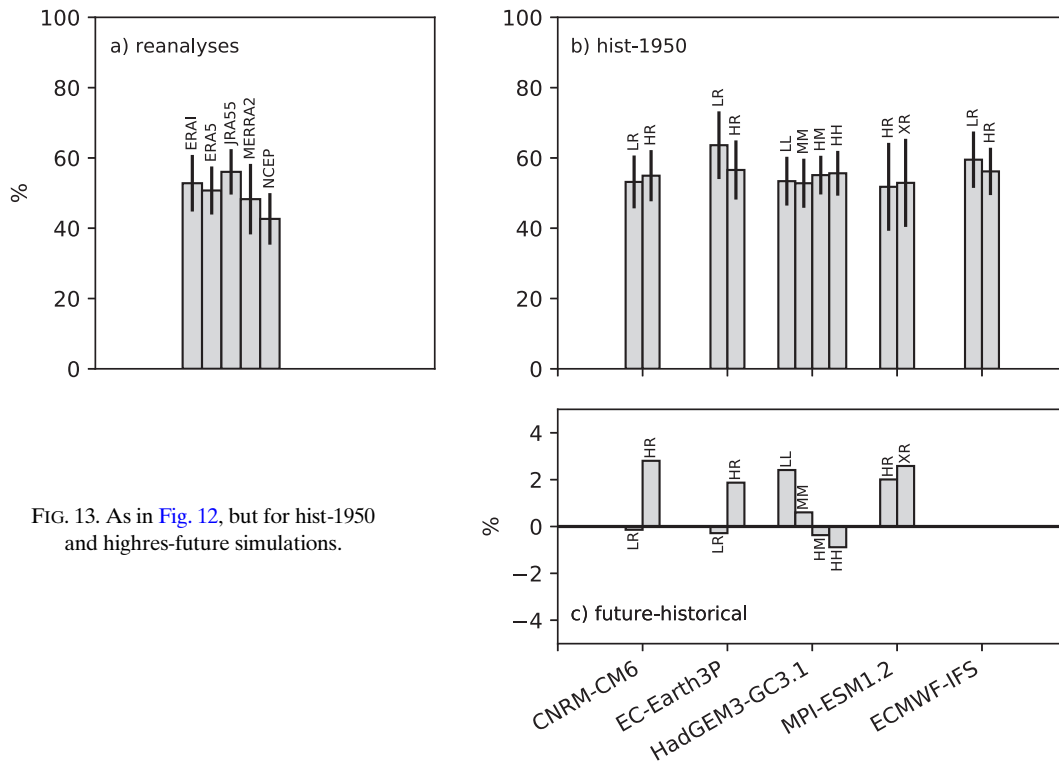
FIG. 13. As in Fig. 12, but for hist-1950 and highres-future simulations.

both atmosphere-only (Fig. 3) and fully coupled (Fig. 4) experiments. In these basins, atmosphere-only simulations exhibit skill of ~0.3 in capturing interannual variability in just the subset of tropical cyclones that undergo ET (Table 4), demonstrating that the skill of these models in simulating all tropical cyclones does not remain throughout the complete cyclone life cycle. Additionally, this level of skill in atmosphere-only simulations is lower than that found for similar-resolution initialized seasonal forecasts (Liu et al. 2018). For the other basins—the northern Indian Ocean and Southern Hemisphere—frequencies simulated by high-resolution models overestimate reanalyses. ET percent, however, is similar between low- and high-resolution simulations, indicating that the resolution sensitivity of ET is driven by that of tropical cyclone frequency, not by an enhancement of environmental conditions conducive to ET. The seasonal cycle of ET is reproduced by most models, with both the seasonal timing and the magnitude of the seasonal peak simulated more correctly at high resolution, but the impact of increased atmospheric resolution is model dependent.

In general, PRIMAVERA models show clearer intermodel agreement on the climate change response of ET frequency than on the response of intensity-related metrics. For most basins, models simulate a frequency decrease in response to climate change, except over the North Atlantic, where an increase is projected (Fig. 2). The magnitude of the North Atlantic response is larger in atmosphere-only simulations than in fully coupled integrations and is enhanced by increasing atmospheric model resolution, although interannual variability is pronounced (Fig. 3 and Fig. 4). A significant positive trend in the ensemble-mean fraction of North Atlantic ET events occurring during

August–November is found over the period 1950–2050 at high resolution, indicating long-term change in ET seasonality in this basin, but no secular seasonality change is simulated in the western North Pacific (Fig. 5). North Atlantic seasonality change may result in a higher proportion of tropical cyclones encountering the midlatitude environment during the part of the seasonal cycle when, climatologically, baroclinicity is highest (Hoskins and Hodges 2019). Opposing future ET responses between the North Atlantic and western North Pacific are potentially underpinned by changes in low-level, pre-ET warm-core structures, which strengthen in response to climate change in the North Atlantic but undergo little change in the western North Pacific (Figs. 6 and 7). Comparing atmosphere-only with fully coupled simulations, the North Atlantic track density response to climate change is more muted in the fully coupled experiment, which is consistent with a less pronounced climate change response of pre-ET structures simulated by coupled models. Simulations with higher-resolution, storm-resolving models will open opportunities to further study realistically deep warm-core cyclones.

Globally, simulated warm-core, pre-ET intensity distributions improve with resolution in most models in both atmosphere-only and fully coupled experiments, better resembling reanalyses (Figs. 10 and 11). Simulated cold-core, post-ET intensity distributions exhibit little sensitivity to resolution across models. Globally, models simulate no clear climate change response of pre- or post-ET intensity distributions, suggesting that, if a signal exists, extending simulations beyond 2050 may be required. Under highresSST-future forcing, some models show decreasing warm-core and increasing cold-core intensities for storms < 17 m s^{-1}, but the opposite response for storms ≥ 17 m s^{-1}.
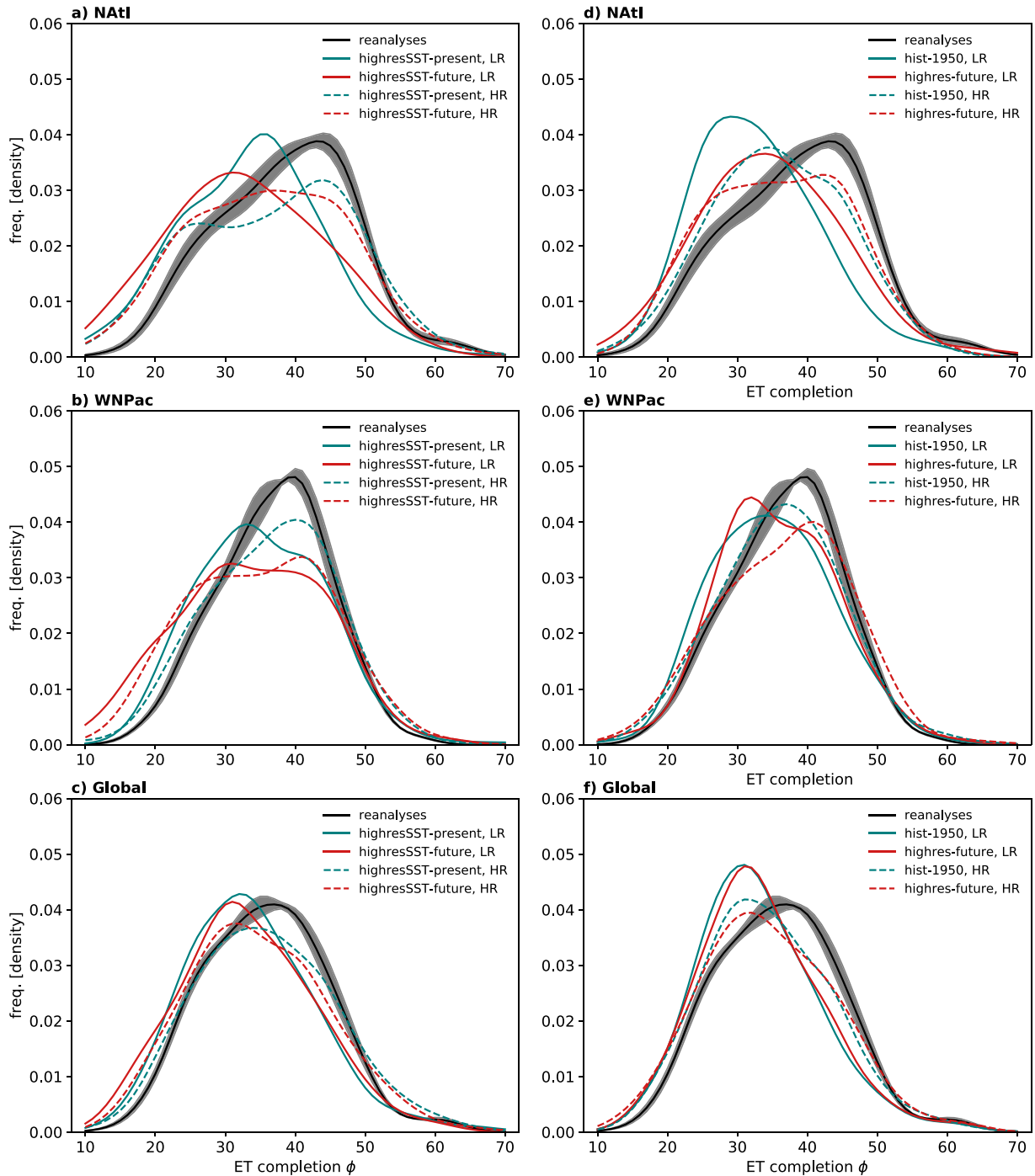
FIG. 14. Ensemble-mean frequency distributions of ET-completion latitude for low- (solid lines) and high-resolution (dashed lines) simulations, for both 1950–2014 (teal) and 2015–50 (red). Results are shown for (a)–(c) atmosphere-only and (d)–(f) fully coupled experiments for the North Atlantic basin (NAtl), western North Pacific basin (WNPac), and all global basins combined. LR and HR denote low- and high-resolution distributions, respectively. Also shown is the multi-reanalysis-mean distribution with shading indicating the standard error for the five reanalyses. Note that frequency is plotted as a function of absolute latitude (ϕ) to combine Northern and Southern Hemisphere results in (c) and (f).

However, this is not reproduced by fully coupled models. Globally, increasing resolution increases the proportion of simulated post-ET reintensifications to approximately match reanalyses, but not in all models. Climate change responses are not significant with respect to historical interannual variability and are model-dependent (Figs. 12 and 13).

The role of model resolution is becoming clearer, but uncertainties remain. Recent analysis of tropical cyclones in the

PRIMAVERA simulations (Roberts et al. 2020b) has shown that the high-resolution atmosphere-only models, which typically have lower wind speed biases, show either reduced future wind speeds or no change. Fully coupled models with the smallest historical biases simulate either no change in future wind speeds or increases of only a few percent. These models therefore project weaker intensity responses to climate change compared with other studies (Knutson et al. 2020). One potential factor is the simplifying aspects of the HighResMIP protocol that are necessary to isolate the role of model resolution, particularly the standardized aerosol forcing and use of a single set of SST and sea ice boundary conditions shared across models (Haarsma et al. 2016). For ET, the climate change responses of pre- and post-ET intensity analyzed in this study are largely model dependent, with models exhibiting little systematic change between atmospheric resolutions of ~100 and ~25 km. This suggests that these disparate responses are due to differences in model formulation, but a larger ensemble of models is likely needed to assess this fully. For post-ET reintensification, increasing atmospheric resolution appears to result in more consistent model behavior, but resolution remains a key research issue because several models still underestimate tropical cyclone intensities at ~25-km grid spacing (Roberts et al. 2020a) and further improvements are anticipated by increasing resolution to at least 10 km (Haarsma 2021; Judt et al. 2021). To obtain samples of ET events comparable to this study, however, running sufficiently long simulations (and/or a sufficiently large ensemble) at these storm-resolving resolutions, even without coupling to an ocean model, remains a significant computational challenge (Roberts et al. 2020b).

Additional outstanding questions and uncertainties remain. A poleward expansion of Hadley circulation termini is projected in a warmer climate (Lu et al. 2007), which implies meridional shifts in tropical storm tracks (Sharmila and Walsh 2018; Studholme and Gulev 2018). However, the impacts of this large-scale change on the spatial distribution and frequency of ET are equivocal. The poleward expansion of regions conducive to tropical cyclone genesis and development that results from an increase in Hadley cell width will reduce the mean displacement required for tropical cyclones to reach the midlatitude baroclinic zone, increasing the likelihood of ET. However, a poleward shift of the midlatitude storm track in response to warming has been projected (Bengtsson et al. 2006), which in turn shifts environmental conditions conducive to extratropical transition poleward, potentially offsetting Hadley-driven changes. Here, we find minimal changes in ET-completion latitude out to 2050 (Fig. 14), suggesting cancellation in the net effect of these competing large-scale changes. Further work is needed to establish the time of emergence of any meridional shift and will require dedicated studies, exploring a range of climate change scenarios with models run at resolutions sufficiently high to adequately represent both tropical cyclones and ET—at least 25 km, according to our results.

This study provides evidence that pre-ET cyclone intensity and warm-core strength exert influence over future changes in ET statistics and seasonality. Analysis of higher-resolution and storm-resolving models (at least 10 km) will help establish whether these results hold true for models able to reproduce more realistic tropical cyclone maximum intensities, including rapidly intensifying systems. Additionally, there is a need to contextualize future projections of ET, accounting for natural variability, and in particular the roles of regional (e.g., Atlantic multidecadal variability) and global (i.e., El Niño–Southern Oscillation) modes of variability on ET frequency. Dedicated sensitivity experiments will be required, and such a study is forthcoming for the North Atlantic, where this work has identified future changes that are important and often unique to this basin. Finally, investigation of secular change in ET seasonality, as seen in the North Atlantic in this study, will be important globally because future modification to the interval between the seasonal maximum of ET occurrence and wintertime storminess may engender considerable changes in risk for populous midlatitude regions.

REFERENCES

Arnott, J. M., J. L. Evans, and F. Chiaromonte, 2004: Characterization of extratropical transition using cluster analysis. *Mon. Wea. Rev.*, **132**, 2916–2937, https://doi.org/10.1175/MWR2836.1.

Baatsen, M., R. J. Haarsma, A. J. van Delden, and H. de Vries, 2015: Severe autumn storms in future western Europe with a warmer Atlantic Ocean. *Climate Dyn.*, **45**, 949–964, https://doi.org/10.1007/s00382-014-2329-8.

Baker, A. J., K. I. Hodges, R. K. H. Schiemann, and P. L. Vidale, 2021: Historical variability and lifecycles of North Atlantic midlatitude cyclones originating in the tropics. *J. Geophys. Res. Atmos.* **126**, e2020JD033924, https://doi.org/10.1029/2020JD033924.

Balaguru, K., S. Taraphdar, L. R. Leung, G. R. Foltz, and J. A. Knaff, 2014: Cyclone–cyclone interactions through the ocean pathway. *Geophys. Res. Lett.*, **41**, 6855–6862, https://doi.org/10.1002/2014GL061489.

Barcikowska, M., F. Feser, and H. von Storch, 2012: Usability of best track data in climate statistics in the western North Pacific. *Mon. Wea. Rev.*, **140**, 2818–2830, https://doi.org/10.1175/MWR-D-11-00175.1.

Bengtsson, L., K. I. Hodges, and E. Roeckner, 2006: Storm tracks and climate change. *J. Climate*, **19**, 3518–3543, https://doi.org/10.1175/JCLI3815.1.

Bieli, M., S. J. Camargo, A. H. Sobel, J. L. Evans, and T. Hall, 2019: A global climatology of extratropical transition. Part I: Characteristics across basins. *J. Climate*, **32**, 3557–3582, https://doi.org/10.1175/JCLI-D-17-0518.1.

——, A. H. Sobel, S. J. Camargo, H. Murakami, and G. A. Vecchi, 2020: Application of the cyclone phase space to extratropical transition in a global climate model. *J. Adv. Model. Earth Syst.*, **12**, e2019MS001878, https://doi.org/10.1029/2019MS001878.

Blake, E. S., and Coauthors, 2013: Hurricane Sandy (AL182012). National Hurricane Center Tropical Cyclone Rep., 157 pp., https://www.nhc.noaa.gov/data/tcr/AL182012_Sandy.pdf.

Chang, E. K. M., and Y. Guo, 2007: Is the number of North Atlantic tropical cyclones significantly underestimated prior to the availability of satellite observations? *Geophys. Res. Lett.*, **34**, L14801, https://doi.org/10.1029/2007GL030169.

Chu, J.-H., C. R. Sampson, A. S. Levine, and E. Fukada, 2002: The Joint Typhoon Warning Center tropical cyclone best-tracks, 1945–2000. United States Naval Research Laboratory, NRL/MR/7540-02-16, https://www.metoc.navy.mil/jtwc/products/best-tracks/tc-bt-report.html.

Davis, C. A., 2018: Resolving tropical cyclone intensity in models. *Geophys. Res. Lett.*, **45**, 2082–2087, https://doi.org/10.1002/2017GL076966.

Dee, D. P., and Coauthors, 2011: The ERA-Interim reanalysis: Configuration and performance of the data assimilation system. *Quart. J. Roy. Meteor. Soc.*, **137**, 553–597, https://doi.org/10.1002/qj.828.

Dekker, M. M., R. J. Haarsma, H. de Vries, M. Baatsen, and A. J. van Delden, 2018: Characteristics and development of European cyclones with tropical origin in reanalysis data. *Climate Dyn.*, **50**, 445–455, https://doi.org/10.1007/s00382-017-3619-8.

Delgado, S., C. W. Landsea, and H. Willoughby, 2018: Reanalysis of the 1954–63 Atlantic hurricane seasons. *J. Climate*, **31**, 4177–4192, https://doi.org/10.1175/JCLI-D-15-0537.1.

Evans, C., and Coauthors, 2017: The extratropical transition of tropical cyclones. Part I: Cyclone evolution and direct impacts. *Mon. Wea. Rev.*, **145**, 4317–4344, https://doi.org/10.1175/MWR-D-17-0027.1.

Grams, C. M., and S. R. Blumer, 2015: European high-impact weather caused by the downstream response to the extratropical transition of North Atlantic Hurricane Katia (2011). *Geophys. Res. Lett.*, **42**, 8738–8748, https://doi.org/10.1002/2015GL066253.

Gutjahr, O., D. Putrasahan, K. Lohmann, J. H. Jungclaus, J. S. von Storch, N. Brüggemann, H. Haak, and A. Stössel, 2019: Max Planck Institute Earth System Model (MPI-ESM1.2) for the High-Resolution Model Intercomparison Project (HighResMIP). *Geosci. Model Dev.*, **12**, 3241–3281, https://doi.org/10.5194/gmd-12-3241-2019.

Haarsma, R., 2021: European windstorm risk of post-tropical cyclones and the impact of climate change. *Geophys. Res. Lett.*, **48**, e2020GL091483, https://doi.org/10.1029/2020GL091483.

——, W. Hazeleger, C. Severijns, H. de Vries, A. Sterl, R. Bintanja, G. J. Oldenborgh, and H. W. Brink, 2013: More hurricanes to hit western Europe due to global warming. *Geophys. Res. Lett.*, **40**, 1783–1788, https://doi.org/10.1002/grl.50360.

——, and Coauthors, 2016: High Resolution Model Intercomparison Project (HighResMIP v1.0) for CMIP6. *Geosci. Model Dev.*, **9**, 4185–4208, https://doi.org/10.5194/gmd-9-4185-2016.

——, and Coauthors, 2020: HighResMIP versions of EC-Earth: EC-Earth3P and EC-Earth3P-HR—Description, model computational performance and basic validation. *Geosci. Model Dev.*, **13**, 3507–3527, https://doi.org/10.5194/gmd-13-3507-2020.

Hagen, A. B., D. Strahan-Sakoskie, and C. Luckett, 2012: A reanalysis of the 1944–53 Atlantic hurricane seasons—The first decade of aircraft reconnaissance. *J. Climate*, **25**, 4441–4460, https://doi.org/10.1175/JCLI-D-11-00419.1.

Harr, P. A., D. Anwender, and S. C. Jones, 2008: Predictability associated with the downstream impacts of the extratropical transition of tropical cyclones: Methodology and a case study of Typhoon Nabi (2005). *Mon. Wea. Rev.*, **136**, 3205–3225, https://doi.org/10.1175/2008MWR2248.1.

Hart, R. E., 2003: A cyclone phase space derived from thermal wind and thermal asymmetry. *Mon. Wea. Rev.*, **131**, 585–616, https://doi.org/10.1175/1520-0493(2003)131<0585:ACPSDF>2.0.CO;2.

——, and J. L. Evans, 2001: A climatology of the extratropical transition of Atlantic tropical cyclones. *J. Climate*, **14**, 546–564, https://doi.org/10.1175/1520-0442(2001)014<0546:ACOTET>2.0.CO;2.

——, ——, and C. Evans, 2006: Synoptic composites of the extratropical transition life cycle of North Atlantic tropical cyclones: Factors determining posttransition evolution. *Mon. Wea. Rev.*, **134**, 553–578, https://doi.org/10.1175/MWR3082.1.

Hersbach, H., and Coauthors, 2020: The ERA5 global reanalysis. *Quart. J. Roy. Meteor. Soc.*, **146**, 1999–2049, https://doi.org/10.1002/qj.3803.

Hodges, K. I., 1995: Feature tracking on the unit sphere. *Mon. Wea. Rev.*, **123**, 3458–3465, https://doi.org/10.1175/1520-0493(1995)123<3458:FTOTUS>2.0.CO;2.

——, 1996: Spherical nonparametric estimators applied to the UGAMP model integration for AMIP. *Mon. Wea. Rev.*, **124**, 2914–2932, https://doi.org/10.1175/1520-0493(1996)124<2914:SNEATT>2.0.CO;2.

——, 1999: Adaptive constraints for feature tracking. *Mon. Wea. Rev.*, **127**, 1362–1373, https://doi.org/10.1175/1520-0493(1999)127<1362:ACFFT>2.0.CO;2.

——, A. Cobb, and P. L. Vidale, 2017: How well are tropical cyclones represented in reanalysis datasets? *J. Climate*, **30**, 5243–5264, https://doi.org/10.1175/JCLI-D-16-0557.1.

Hoskins, B. J., and P. J. Valdes, 1990: On the existence of storm-tracks. *J. Atmos. Sci.*, **47**, 1854–1864, https://doi.org/10.1175/1520-0469(1990)047<1854:OTEOST>2.0.CO;2.

——, and K. I. Hodges, 2019: The annual cycle of Northern Hemisphere storm tracks. Part I: Seasons. *J. Climate*, **32**, 1743–1760, https://doi.org/10.1175/JCLI-D-17-0870.1.

Ito, R., T. Takemi, and O. Arakawa, 2016: A possible reduction in the severity of typhoon wind in the northern part of Japan under global warming: A case study. *SOLA*, **12**, 100–105, https://doi.org/10.2151/sola.2016-023.

Jones, S. C., and Coauthors, 2003: The extratropical transition of tropical cyclones: Forecast challenges, current understanding, and future directions. *Wea. Forecasting*, **18**, 1052–1092, https://doi.org/10.1175/1520-0434(2003)018<1052:TETOTC>2.0.CO;2.

Judt, F., and Coauthors, 2021: Tropical cyclones in global storm-resolving models. *J. Meteor. Soc. Japan*, **99**, 579–602, https://doi.org/10.2151/jmsj.2021-029.

Jung, C., and G. M. Lackmann, 2021: The response of extratropical transition of tropical cyclones to climate change: Quasi-idealized numerical experiments. *J. Climate*, **34**, 4361–4381, https://doi.org/10.1175/JCLI-D-20-0543.1.

Keller, J. H., and Coauthors, 2019: The extratropical transition of tropical cyclones. Part II: Interaction with the midlatitude flow, downstream impacts, and implications for predictability. *Mon. Wea. Rev.*, **147**, 1077–1106, https://doi.org/10.1175/MWR-D-17-0329.1.

Kitabatake, N., 2011: Climatology of extratropical transition of tropical cyclones in the western North Pacific defined by using cyclone phase space. *J. Meteor. Soc. Japan*, **89**, 309–325, https://doi.org/10.2151/jmsj.2011-402.

Klaver, R., R. Haarsma, P. L. Vidale, and W. Hazeleger, 2020: Effective resolution in high resolution global atmospheric models for climate studies. *Atmos. Sci. Lett.*, **21**, e952, https://doi.org/10.1002/asl.952.

Klein, P. M., P. A. Harr, and R. L. Elsberry, 2002: Extratropical transition of western North Pacific tropical cyclones: Midlatitude and tropical cyclone contributions to reintensification. *Mon. Wea. Rev.*, **130**, 2240–2259, https://doi.org/10.1175/1520-0493(2002)130<2240:ETOWNP>2.0.CO;2.

Knutson, T., and Coauthors, 2020: Tropical cyclones and climate change assessment: Part II: Projected response to anthropogenic warming. *Bull. Amer. Meteor. Soc.*, **101**, E303–E322, https://doi.org/10.1175/BAMS-D-18-0194.1.

Kobayashi, S., and Coauthors, 2015: The JRA-55 Reanalysis: General specifications and basic characteristics. *J. Meteor. Soc. Japan*, **93**, 5–48, https://doi.org/10.2151/jmsj.2015-001.

Kofron, D. E., E. A. Ritchie, and J. S. Tyo, 2010: Determination of a consistent time for the extratropical transition of tropical cyclones. Part I: Examination of existing methods for finding "ET time." *Mon. Wea. Rev.*, **138**, 4328–4343, https://doi.org/10.1175/2010MWR3180.1.

Kossin, J. P., K. R. Knapp, D. J. Vimont, R. J. Murnane, and B. A. Harper, 2007: A globally consistent reanalysis of hurricane variability and trends. *Geophys. Res. Lett.*, **34**, L04815, https://doi.org/10.1029/2006GL028836.

Lanzante, J. R., 2019: Uncertainties in tropical-cyclone translation speed. *Nature*, **570**, E6–E15, https://doi.org/10.1038/s41586-019-1223-2.

Laurila, T. K., V. A. Sinclair, and H. Gregow, 2019: The extratropical transition of Hurricane Debby (1982) and the subsequent development of an intense windstorm over Finland. *Mon. Wea. Rev.*, **148**, 377–401, https://doi.org/10.1175/MWR-D-19-0035.1.

Liu, M., G. A. Vecchi, J. A. Smith, and H. Murakami, 2017: The present-day simulation and twenty-first-century projection of the climatology of extratropical transition in the North Atlantic. *J. Climate*, **30**, 2739–2756, https://doi.org/10.1175/JCLI-D-16-0352.1.

——, ——, ——, ——, R. Gudgel, and X. Yang, 2018: Towards dynamical seasonal forecast of extratropical transition in the North Atlantic. *Geophys. Res. Lett.*, **45**, 12 602–12 609, https://doi.org/10.1029/2018GL079451.

Lu, J., G. A. Vecchi, and T. Reichler, 2007: Expansion of the Hadley cell under global warming. *Geophys. Res. Lett.*, **34**, L06805, http://dx.doi.org/10.1029/2006GL028443.

Manganello, J. V., B. A. Cash, K. I. Hodges, and J. L. Kinter, 2019: Seasonal forecasts of North Atlantic tropical cyclone activity in the North American Multi-Model Ensemble. *Climate Dyn.*, **53**, 7169–7184, https://doi.org/10.1007/s00382-017-3670-5.

Michaelis, A. C., and G. M. Lackmann, 2019: Climatological changes in the extratropical transition of tropical cyclones in high-resolution global simulations. *J. Climate*, **32**, 8733–8753, https://doi.org/10.1175/JCLI-D-19-0259.1.

——, and ——, 2021: Storm-scale dynamical changes of extratropical transition events in present-day and future high-resolution global simulations. *J. Climate*, **34**, 5037–5062, https://doi.org/10.1175/JCLI-D-20-0472.1.

Molod, A., L. Takacs, M. Suarez, and J. Bacmeister, 2015: Development of the GEOS-5 atmospheric general circulation model: Evolution from MERRA to MERRA2. *Geosci. Model Dev.*, **8**, 1339–1356, https://doi.org/10.5194/gmd-8-1339-2015.

Moon, I.-J., S.-H. Kim, and J. C. L. Chan, 2019: Climate change and tropical cyclone trend. *Nature*, **570**, E3–E5, https://doi.org/10.1038/s41586-019-1222-3.

Moreno-Chamarro, E., and Coauthors, 2022: Impact of increased resolution on long-standing biases in HighResMIP-PRIMAVERA climate models. *Geosci. Model Dev.*, **15**, 269–289, https://doi.org/10.5194/gmd-15-269-2022.

Murakami, H., 2014: Tropical cyclones in reanalysis data sets. *Geophys. Res. Lett.*, **41**, 2133–2141, https://doi.org/10.1002/2014GL059519.

Rantanen, M., J. Räisänen, V. A. Sinclair, J. Lento, and H. Järvinen, 2020: The extratropical transition of Hurricane Ophelia (2017) as diagnosed with a generalized omega equation and vorticity equation. *Tellus*, **72A** (1), 1–26, https://doi.org/10.1080/16000870.2020.1721215.

Roberts, C. D., R. Senan, F. Molteni, S. Boussetta, M. Mayer, and S. P. E. Keeley, 2018: Climate model configurations of the ECMWF Integrated Forecasting System (ECMWF-IFS cycle 43r1) for HighResMIP. *Geosci. Model Dev.*, **11**, 3681–3712, https://doi.org/10.5194/gmd-11-3681-2018.

Roberts, M. J., and Coauthors, 2015: Tropical cyclones in the UPSCALE ensemble of high-resolution global climate models. *J. Climate*, **28**, 574–596, https://doi.org/10.1175/JCLI-D-14-00131.1.

——, and Coauthors, 2019: Description of the resolution hierarchy of the global coupled HadGEM3-GC3.1 model as used in CMIP6 HighResMIP experiments. *Geosci. Model Dev.*, **12**, 4999–5028, https://doi.org/10.5194/gmd-12-4999-2019.

——, and Coauthors, 2020a: Impact of model resolution on tropical cyclone simulation using the HighResMIP–PRIMAVERA multimodel ensemble. *J. Climate*, **33**, 2557–2583, https://doi.org/10.1175/JCLI-D-19-0639.1.

——, and Coauthors, 2020b: Projected future changes in tropical cyclones using the CMIP6 HighResMIP multimodel ensemble. *Geophys. Res. Lett.*, **47**, e2020GL088662, https://doi.org/10.1029/2020GL088662.

Saha, S., and Coauthors, 2014: The NCEP Climate Forecast System version 2. *J. Climate*, **27**, 2185–2208, https://doi.org/10.1175/JCLI-D-12-00823.1.

Sainsbury, E. M., R. K. H. Schiemann, K. I. Hodges, L. C. Shaffrey, A. J. Baker, and K. T. Bhatia, 2020: How important are post-tropical cyclones for European windstorm risk? *Geophys. Res. Lett.*, **47**, e2020GL089853, https://doi.org/10.1029/2020GL089853.

Schreck, C. J., III, K. R. Knapp, and J. P. Kossin, 2014: The impact of best track discrepancies on global tropical cyclone climatologies using IBTrACS. *Mon. Wea. Rev.*, **142**, 3881–3899, https://doi.org/10.1175/MWR-D-14-00021.1.

Sharmila, S., and K. J. E. Walsh, 2018: Recent poleward shift of tropical cyclone formation linked to Hadley cell expansion. *Nat. Climate Change*, **8**, 730–736, https://doi.org/10.1038/s41558-018-0227-5.

Stewart, S. R., 2018: Hurricane Ophelia (AL172017). National Hurricane Center Tropical Cyclone Rep., 32 pp., www.nhc.noaa.gov/data/tcr/AL172017_Ophelia.pdf.

Strachan, J., P. L. Vidale, K. Hodges, M. Roberts, and M.-E. Demory, 2013: Investigating global tropical cyclone activity with a hierarchy of AGCMs: The role of model resolution. *J. Climate*, **26**, 133–152, https://doi.org/10.1175/JCLI-D-12-00012.1.

Studholme, J., and S. Gulev, 2018: Concurrent changes to Hadley circulation and the meridional distribution of tropical cyclones. *J. Climate*, **31**, 4367–4389, https://doi.org/10.1175/JCLI-D-17-0852.1.

——, K. I. Hodges, and C. M. Brierley, 2015: Objective determination of the extratropical transition of tropical cyclones in the Northern Hemisphere. *Tellus*, **67A**, 24474, https://doi.org/10.3402/tellusa.v67.24474.

——, A. V. Fedorov, S. K. Gulev, K. Emanuel, and K. Hodges, 2022: Poleward expansion of tropical cyclone latitudes in warming climates. *Nat. Geosci.*, **15**, 14–28, https://doi.org/10.1038/s41561-021-00859-1.

Vannière, B., and Coauthors, 2020: The moisture budget of tropical cyclones in HighResMIP models: Large-scale environmental balance and sensitivity to horizontal resolution. *J. Climate*, **33**, 8457–8474, https://doi.org/10.1175/JCLI-D-19-0999.1.

Vecchi, G. A., and T. R. Knutson, 2008: On estimates of historical North Atlantic tropical cyclone activity. *J. Climate*, **21**, 3580–3600, https://doi.org/10.1175/2008JCLI2178.1.

——, and ——, 2011: Estimating annual numbers of Atlantic hurricanes missing from the HURDAT database (1878–1965) using ship track density. *J. Climate*, **24**, 1736–1746, https://doi.org/10.1175/2010JCLI3810.1.

——, and Coauthors, 2019: Tropical cyclone sensitivities to CO_2 doubling: Roles of atmospheric resolution, synoptic variability and background climate changes. *Climate Dyn.*, **53**, 5999–6033, https://doi.org/10.1007/s00382-019-04913-y.

Velden, C., and Coauthors, 2006: The Dvorak tropical cyclone intensity estimation technique: A satellite-based method that has endured for over 30 years. *Bull. Amer. Meteor. Soc.*, **87**, 1195–1210, https://doi.org/10.1175/BAMS-87-9-1195.

Vidale, P. L., and Coauthors, 2021: Impact of stochastic physics and model resolution on the simulation of tropical cyclones in climate GCMs. *J. Climate*, **34**, 4315–4341, https://doi.org/10.1175/JCLI-D-20-0507.1.

Voldoire, A., and Coauthors, 2019: Evaluation of CMIP6 DECK experiments with CNRM-CM6-1. *J. Adv. Model. Earth Syst.*, **11**, 2177–2213, https://doi.org/10.1029/2019MS001683.

Weinkle, J., C. Landsea, D. Collins, R. Musulin, R. P. Crompton, P. J. Klotzbach, and R. Pielke, 2018: Normalized hurricane damage in the continental United States 1900–2017. *Nat. Sustainability*, **1**, 808–813, https://doi.org/10.1038/s41893-018-0165-2.

Williams, K. D., and Coauthors, 2018: The Met Office global coupled model 3.0 and 3.1 (GC3.0 and GC3.1) configurations. *J. Adv. Model. Earth Syst.*, **10**, 357–380, https://doi.org/10.1002/2017MS001115.

Wood, K. M., and E. A. Ritchie, 2014: A 40-year climatology of extratropical transition in the eastern North Pacific. *J. Climate*, **27**, 5999–6015, https://doi.org/10.1175/JCLI-D-13-00645.1.

Zarzycki, C. M., D. R. Thatcher, and C. Jablonowski, 2017: Objective tropical cyclone extratropical transition detection in high-resolution reanalysis and climate model data. *J. Adv. Model. Earth Syst.*, **9**, 130–148, https://doi.org/10.1002/2016MS000775.

Zhu, X., L. Wu, and Q. Wang, 2018: Extratropical transition and re-intensification of Typhoon Toraji (2001): Large-scale circulations, structural characteristics, and mechanism analysis. *J. Ocean Univ. China*, **17**, 461–476, https://doi.org/10.1007/s11802-018-3376-2.